International Journal of Nanomedicine

Dovepress
open access to scientific and medical research

Open Access Full Text Article

REVIEW

Gold nanoparticles enlighten the future of cancer theranostics

International Journal of Nanomedicine downloaded from https://www.dovepress.com/ on 27-Aug-2022
For personal use only.

Jianfeng Guo[1]
Kamil Rahme[2–4]
Yan He[1]
Lin-Lin Li[5]
Justin D Holmes[3,4]
Caitriona M O'Driscoll[6]

[1]School of Pharmaceutical Sciences, Jilin University, Changchun, China; [2]Department of Sciences, Faculty of Natural and Applied Science, Notre Dame University (Louaize), Zouk Mosbeh, Lebanon; [3]Department of Chemistry, Tyndall National Institute, University College Cork, Cork, [4]AMBER@CRANN, Trinity College Dublin, Dublin, Ireland; [5]The First Hospital of Jilin University, Changchun, China; [6]Pharmacodelivery Group, School of Pharmacy, University College Cork, Cork, Ireland

Correspondence: Jianfeng Guo
School of Pharmaceutical Sciences, Jilin University, 1266, Fujin Road, Changchun 130021, China
Tel +86 431 8561 9716
Fax +86 431 8561 9252
Email jguo@jlu.edu.cn

Caitriona M O'Driscoll
Pharmacodelivery Group, School of Pharmacy, University College Cork, College Road, Cork, Ireland
Tel +353 21 490 1396
Fax +353 21 490 1656
Email caitriona.odriscoll@ucc.ie

Abstract: Development of multifunctional nanomaterials, one of the most interesting and advanced research areas in the field of nanotechnology, is anticipated to revolutionize cancer diagnosis and treatment. Gold nanoparticles (AuNPs) are now being widely utilized in bioimaging and phototherapy due to their tunable and highly sensitive optical and electronic properties (the surface plasmon resonance). As a new concept, termed "theranostics," multifunctional AuNPs may contain diagnostic and therapeutic functions that can be integrated into one system, thereby simultaneously facilitating diagnosis and therapy and monitoring therapeutic responses. In this review, the important properties of AuNPs relevant to diagnostic and phototherapeutic applications such as structure, shape, optics, and surface chemistry are described. Barriers for translational development of theranostic AuNPs and recent advances in the application of AuNPs for cancer diagnosis, photothermal, and photodynamic therapy are discussed.

Keywords: multifunctional gold nanoparticles, cancer bioimaging, cancer photothermal and photodynamic therapy

Introduction

Cancer, one of the leading causes of mortality worldwide, has caused approximately 8.8 million deaths in 2015 (www.who.int). The number of people who are diagnosed with this malignancy is expected to rise to 22 million annually in the next 2 decades (www.who.int). Despite the increased knowledge about the causes of cancer and the improved interventions to prevent and manage the disease, survival rates are still low mainly due to the delay in diagnosis, lack of effective therapeutics, and high incidence of relapse.

As an emerging concept that facilitates simultaneous diagnosis and treatment, the implementation of theranostic nanomaterials (ie, metal and silica nanoparticles [NPs], liposomes, dendrimers, quantum dots, and carbon nanotubes) has great potential for improved cancer treatment and reduced side effects.[1–6] Among these, gold NPs (AuNPs) exhibit favorable physical properties and tailored surface functionalization, providing a potential platform for developing cancer theranostics. This review provides a comprehensive overview of AuNPs as emerging nanomaterials for future cancer theranostics. In this regard, the key physicochemical properties of AuNPs such as structure, shape, optics, and surface chemistry are discussed. In addition, various AuNP-based diagnostic and phototherapeutic strategies under investigation are critically evaluated, with a particular emphasis on those developed to overcome delivery barriers.

submit your manuscript | www.dovepress.com
Dovepress
http://dx.doi.org/10.2147/IJN.S140772

© 2017 Guo et al. This work is published and licensed by Dove Medical Press Limited. The full terms of this license are available at https://www.dovepress.com/terms.php and incorporate the Creative Commons Attribution – Non Commercial (unported, v3.0) License (http://creativecommons.org/licenses/by-nc/3.0/). By accessing the work you hereby accept the Terms. Non-commercial uses of the work are permitted without any further permission from Dove Medical Press Limited, provided the work is properly attributed. For permission for commercial use of this work, please see paragraphs 4.2 and 5 of our Terms (https://www.dovepress.com/terms.php).

Key properties of AuNPs for diagnosis and phototherapy

Types of AuNPs

Colloidal AuNPs were first produced in 1857 by Faraday,[7] where the "fine particles" were formed from the reduction of gold chloride by phosphorus and the stabilization of AuNPs by carbon disulfide. In 1951, Turkevich et al[8] reported the formation of colloidal AuNPs using trisodium citrate ($HOC(COONa)(CH_2COONa)_2$) to reduce tetrachloroauric acid (gold [III] chloride [$HAuCl_4$]) in water, and later Frens[9] improved the formation using a slightly modified method. Recently, AuNPs have been produced with various sizes and shapes (ie, gold nanospheres, nanorods, nanocages, nanoshells, and nanostars), which are dependent upon the synthetic methods adopted for their preparation (Figure 1; a summary of synthetic approaches to obtain various gold nanostructures has been described previously).[10–14]

A

AuNPs	Theranostic applications
Au Nanosphere (2–100 nm)	• Cell imaging (visible lights) • PTT (visible lights) • Delivery of therapeutic cargos (ie, photosensitizers)
Au Nanorod (10–100 nm)	• Tumour imaging (enhanced radiative property; NIR) • PTT (enhanced nonradiative property; NIR) • Delivery of therapeutic cargos (ie, photosensitizers)
Au Silica Nanoshell (100 nm)	• Tumour imaging (enhanced radiative property; NIR) • PTT (enhanced nonradiative property; NIR) • PDT (unique shape and structure) • Delivery of therapeutic cargos (ie, photosensitizers)
Nanocage (40–50 nm)	• Tumour imaging (enhanced radiative property; NIR) • PTT (enhanced nonradiative property; NIR) • PDT (unique shape and structure) • Delivery of therapeutic cargos (ie, photosensitizers)

B

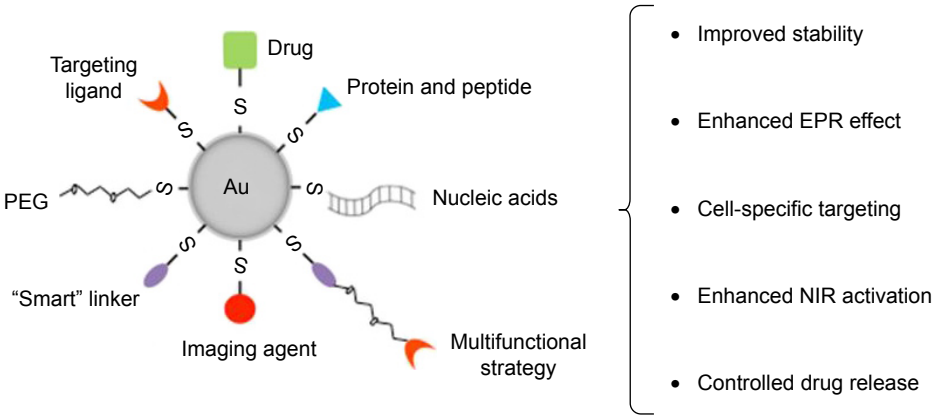

Figure 1 Development of theranostic AuNPs in the treatment of cancer.

Notes: (**A**) Commonly used AuNPs can be categorized depending on the particle shape, including Au nanospheres, nanorods, nanoshells, and nanocages. These AuNPs with tunable optical and electronic properties and easy surface functionalizations have presented great potential for cancer bioimaging, PTT/PDT, and targeted drug delivery. (**B**) Functional components including stealth coating materials, bioresponsive moieties, bioactive targeting ligands, bioimaging agents, and therapeutic cargos can be integrated into one system, to achieve multifunctional AuNPs for future cancer treatment.

Abbreviations: AuNPs, gold nanoparticles; EPR, enhanced penetration and retention; NIR, near-infrared; PDT, photodynamic therapy; PEG, polyethylene glycol; PTT, photothermal therapy.

Gold nanospheres

Gold nanospheres (particle size 2–100 nm) are generally prepared after reducing $HAuCl_4$ with the assistance of different reducing agents under various temperature and pressure. Trisodium citrate (sometimes referred to simply as sodium citrate), for example, is a commonly used reducing and stabilizing agent, which is capable of generating monodisperse gold nanospheres with different particle sizes by adjusting the concentration of citrate.[11]

The seeding growth strategy has been used to improve monodispersity and avoid the formation of large AuNPs with irregular shapes (diameter >50 nm), whereby large spherical AuNPs are produced by reducing $HAuCl_4$ or Au (III)-surfactant complexes onto the surface of preexisting seeds using reducing agents such as hydroxylamine hydrochloride,[15,16] ascorbic acid,[17] 2-mercaptosuccinic acid,[18] hydroquinone,[19] and hydrogen peroxide.[20]

Gold nanorods (GNRs)

GNRs were first synthesized by Foss et al,[21] Martin,[22] and Perez-Juste et al[23] using the template method. They are generally synthesized with a size ranging from 10 nm to 100 nm and an aspect ratio between 1 (sphere) and 7 with a corresponding longitudinal plasmon of ~1,050 nm. However, the yield is low due to the fact that only one monolayer of nanorods is produced using the template approach.

Alternatively, the seed growth method is also used to synthesize GNRs.[23] In this method, gold seeds are prepared by reducing the gold salt with a strong reducing agent (ie, sodium borohydride). These seeds that provide the nucleation sites are subsequently added to the aqueous surfactant media containing the gold salt and the reducing agents (ie, ascorbic acid and hexadecyltrimethylammonium bromide [CTAB]) for the growth steps.[24,25] Additional nucleation during the growth stage can be inhibited by controlling the growth conditions such as 1) the rate of addition of reducing agents to the gold seed and gold salt solution and 2) the reduction potential of reducing agents. As a result, the aspect ratios of nanorods (the ratio of the longer side to the shorter side) can be controlled by using different amounts of gold seeds relative to the precursor.

Gold nanocages

Gold nanocages are hollow nanostructures (particle size ~40–50 nm) which can be prepared with controllable pores on the surface via the galvanic replacement reaction between truncated silver (Ag) nanocubes and $HAuCl_4$.[26] Silver nanostructures with controlled shapes can be generated via the polyol reduction, where $AgNO_3$ is reduced by ethylene glycol to generate Ag atoms followed by nanocrystals or seeds. Silver nanostructures are utilized as the sacrificial template and can be transformed into AuNPs with hollow structures via the galvanic replacement.[26] The molar ratio of Ag to $HAuCl_4$ can be regulated to manipulate the diameter and wall thickness of resultant gold nanocages.[26]

Gold nanoshells

Gold nanoshells are normally composed of dielectric core materials (ie, silica and polystyrene) coated by a thin gold layer. Core materials such as silica and polystyrene have been widely used to provide high stability and monodispersity.[27] These core materials can be tailored by varying the dimensions of the core and/or the shell; normally, the core has a diameter ~100 nm and a thin shell of gold about several nanometers (~1–20 nm).[28,29]

Modification of the core surface with a bifunctional ligand that enhances the shell coverage is a common method for the preparation of gold nanoshells. In the case of silica, the core surface is modified by 3-aminopropyltriethoxysilane (APS) with both ethoxy and amine groups. The ethoxy group binds covalently to silica surface through the hydroxyl group, while the amine group attaches to gold seeds. In addition, bifunctional linkers such as 3-aminopropyltrimethoxysilane (APTMS) and 3-mercaptopropyltrimethoxysilane (MPTMS) have also been used to modify the silica, leading to amino- and thiol-functionalized surfaces that can efficiently attach to gold seeds. As a result, the complete shell is formed by aging the gold attached onto the silica core.[30]

Optical characteristics of AuNPs

It is known that the oscillating electromagnetic field of light induces a collective coherent oscillation of the free electrons (also known as conduction band electrons) of the metal.[31] The amplitude of the oscillation that reaches a maximum at a specific frequency is termed the surface plasmon resonance (SPR).[31] A strong absorption of the incident light is induced by the SPR and can be measured using an ultraviolet (UV)–visible absorption spectrometer.[32] The SPR band of noble metals (ie, gold and silver) is known to be much stronger than other metals.[32] The SPR wavelength of AuNPs can be tuned from the visible to the near-infrared (NIR) region by changing the size, shape, and structure of AuNPs, as theoretically described by the Mie theory.[32]

Two main processes, namely, absorption and scattering, occur when the light passes through matter resulting in the energy loss of electromagnetic wave.[33] The scattered light has the same frequency as the incident light (it is termed as Rayleigh scattering) or a shifted frequency (it is termed as

Raman scattering).[33] AuNPs can significantly enhance the light scattering, ie, five- to six-fold stronger than most strongly absorbing organic dyes and higher than the emission of most strongly fluoresceins,[34] which makes AuNPs very promising imaging and detection platforms for cancer, as described in the "AuNPs for cancer diagnosis" section.

The scattering properties are highly dependent on the size and shape of AuNPs, which are given in the following sections.

Particle size

AuNPs with particle sizes of ~40 nm may be easily detected down to a particle concentration of 10^{-14} M.[35,36] Moreover, the scattering of ~60 nm AuNPs is ~100-fold stronger than the emission of a fluorescein.[36] Likewise, ~70 nm AuNPs can scatter orders of magnitude stronger than that of a polystyrene sphere of the same size.[37] It has been reported that ~30–100 nm AuNPs can be detected under a microscope using dark-field illumination conditions (only the light scattered from indirect illumination of the sample is detected).[38] Recently, Jain et al[34] and Lee and El-Sayed[39] have substantially studied the relationship between the optical absorption/scattering and the size of AuNPs using the Mie theory. They reported that the total extinction of ~20 nm AuNPs was mostly contributed by absorption; when the particle size of AuNPs was ~40 nm, they initiated scattering, and when the particle size was ~80 nm, the extinction of AuNPs was contributed by absorption and scattering in a very similar degree.[34,39] This fact that the ratio of scattering to absorption increases significantly for larger size of particles can guide the development of AuNPs for bioimaging.

Particle shape

The optical properties of AuNPs can also be tuned by shape.[40–42] When the shape of AuNPs is changed from sphere to rod, the SPR will be split into two bands, namely, a strong band in the NIR region and a weak band in the visible region, as predicted by the Gans theory. The strong band, also referred to as the longitudinal band, results from electron oscillations along the long axis. The weak band, also known as the transverse band, is similar to the wavelength of gold nanospheres. Tong et al[43] reported that the longitudinal band of GNRs was red shifted largely by increasing the aspect ratios (length/width), which causes the color change from blue to red. In addition, Lee and El-Sayed[44] have shown that when the aspect ratio of GNRs was increased, light scattering was significantly enhanced.

It is known that the SPR of gold nanocages may be tuned to the NIR region with specified wavelengths.[45] For instance, the particle size of gold nanocages is generally ~50 nm edge width with several nanometer walls and holes for an SPR wavelength of ~800 nm.[46]

Particle composition

It is known that the composition of NPs (particularly semiconductor NPs such as quantum dots) is also able to affect the scattering properties;[47] recently, several studies have focused on the scattering properties dependent on the composition of Au nanocomplexes.[48–50] Jain et al[34] have investigated the scattering properties of the core–shell composition in silica–Au nanoshells using Mie theory and discrete dipole approximation method. Results show that the thicknesses of the core and the shell and the radius ratio of core/shell significantly influenced the optical characteristics such as the resonance wavelength, the extinction cross-section, and the ratio of scattering to absorption.[34] In addition, it was reported that the SPR wavelength of silica–Au nanoshells may be changed by controlling the Au shell thickness; for example, when the shell thickness was decreased from 20 to 5 nm, the SPR was red shifted ~300 nm, which most likely results from the increased coupling between the inner and outer shell surface plasmons for thinner shell particles.[30]

Surface functionalization of AuNPs

The surface chemistry of gold makes AuNPs a promising platform for biomedical applications (Figure 1).[11] Brust et al[51] exploited the high affinity of thiol for gold to produce AuNP-thiolates (Au-S); this was achieved using $HAuCl_4$, thiol, tetraoctylammonium bromide, and $NaBH_4$ in water–toluene and was stabilized via Au-S-stabilizer bonds. These NPs were dispersed in organic solvent and required further phase transfer or ligand exchange to transfer them into water. An essential purification step to remove impurities for use in biological application was also necessary.

In addition, ligands containing amine and phosphine groups, which also have high affinity with the surface of gold, have been used as efficient stabilizing agents.[52] For example, cationic surfactant-free AuNPs (~2–200 nm) have been developed that were synthesized in water using a seed growth method, in the presence of L-cysteine methyl ester hydrochloride ($HSCH_2CH(NH_2)COOCH_3 \cdot HCl$) as a capping agent.[53] Furthermore, Chhour et al[54] have functionalized AuNPs using a group of thiol and amine ligands, including 11-mercaptoundecanoic acid (11-MUDA), 16-mercaptohexadecanoic acid (16-MHDA), polyethylenimine (PEI),

4-mercapto-1-butanol (4-MB), and 11-mercaptoundecyl-tetra (ethylene glycol) (MTEG). These ligands enhanced the AuNP stability and provided different surface functionalities which can influence cell uptake and cytotoxicity.[54] Among them, the 11-MUDA AuNPs were used to monitor the recruitment of monocytes into atherosclerotic plaques in a disease mouse model using X-ray computed tomography (CT), potentially allowing detection of monocyte recruitment in the presence of emerging atherosclerosis therapies.[54] In addition, Liu et al[55] have recently stabilized AuNPs using thiol-polyethylene glycol (SH-PEG) at two different ratios of thiol to PEG (1:1 and 1:2), significantly improving the AuNP stability in biological media. When AuNPs with higher PEG content were intravenously injected, they were found to accumulate in the liver at a lower level relative to counterparts with lower PEG content.[55] These results suggest that when designing AuNPs, a rational ratio between the anchoring group (ie, thiol) and the hydrophilic group (ie, PEG) should be carefully considered, this is important for integrating the properties of NPs in certain bio-related application.

Targeting ligands[56–60] may be modified onto the AuNP surface to specifically deliver therapeutic cargos into tissues and organs. Recently, tumor-targeted mesoporous silica-encapsulated GNRs (GNRs@mSiO$_2$) for chemotherapy and photothermal therapy (PTT) have been developed by Shen et al.[61] In this study, RGD peptides, a targeting ligand for $\alpha_v\beta_3$ integrin receptors that are known to overexpress on several cancer cells, were conjugated to the terminal groups of PEG on GNRs@mSiO$_2$ (namely, pGNRs@mSiO$_2$-RGD). The pGNRs@mSiO$_2$-RGD presented significant stability in bio-environments and efficient loading of doxorubicin (DOX, an antitumor chemotherapeutics). Following the NIR irradiation, the combination of photothermal ablation and DOX-mediated cytotoxicity using pGNRs@mSiO$_2$-RGD resulted in significant tumor reduction in subcutaneous xenografted mice.[61] In addition, it has been reported that PEI-capped AuNPs (Au-PEI) were conjugated with anisamide (AA, which is known to bind to the sigma receptor overexpressed on prostate cancer cells)[62,63] to produce the AA-targeted AuNPs (Au-PEI-AA).[59] As a result, Au-PEI-AA facilitated siRNA uptake into prostate cancer PC-3 cells via binding to the sigma receptor and achieved efficient downregulation of the targeted oncogene.[59]

In addition to the aforementioned stabilizing and targeting ligands, the gold surface can also be modified using several suitable imaging agents, photosensitive molecules, and bioactive/bioresponsive moieties (ie, pH-sensitive linkers, matrix metalloproteinase [MMP]-sensitive linkers, temperature-sensitive linkers, fusogenic/synthetic peptides, and endosomal membrane-disruptive materials) to achieve multifunctional AuNPs for cancer diagnosis and phototherapy, which are discussed in the following sections.

AuNPs for cancer diagnosis

Spectroscopic cancer imaging

For wavelengths >650 and <2,000 nm, the tissue absorption is weak, so the NIR light (wavelength from 700 to 2,500 nm) is normally chosen to image tumor deeply within the body. It is worth noting that the penetration depth of NIR light into tissues is highly dependent on the tissue type, the wavelength, and the condition of the incident beam (ie, the laser power, irradiation time, and time interval).[64–66] For example, it was shown that no penetration was found in the skin, skull, or brain for NIR light with low-power laser; however, 0.45%–2.90% of 810 nm NIR light at high power (10–15 W) was delivered into 3 cm of the aforementioned tissues.[66]

AuNPs on their own may act as an NIR-active imaging probe for cancer detection facilitating whole-body scans due to the unique optical properties. The use of targeted AuNPs as the contrast agent was demonstrated by Sokolov et al,[37] where AuNPs were conjugated with an antibody against the epidermal growth factor receptor (EGFR, it is known to overexpress on many cancers). These AuNP conjugates were used for detecting cancer cells using a scanning confocal microscope in the reflectance mode with a 647 nm laser to excite the SPR of AuNPs; as a result, cells with AuNP conjugates were clearly imaged on a dark background.[37] El-Sayed et al[67] improved the use of AuNPs (~35 nm) as the contrast agent via dark-field microscopy. Following excitation by white light, only the wavelength of light corresponding to the maximum of the SPR of AuNPs was displayed intensely, where a bright image of cells with AuNPs could be seen on a dark background.[67] Moreover, cetuximab (CET, a chimeric monoclonal antibody against the EGFR)-conjugated PEGylated GNRs (CET-pGNRs) was developed for cancer imaging in xenografted mice.[68] The results of in vivo NIR absorption imaging show that specific targeting of CET-pGNRs to the tumor region was evident by a significant increase in the absorption signal. The biodistribution data also show that the amount of AuNPs in tumor tissues from mice injected with CET-pGNRs was eightfold greater than that recorded by nontargeted pGNRs, confirming the results from the NIR absorption imaging. These indicate that CET-pGNRs can specifically target tumor

tissues with high specificity and provide a potential tool for NIR-based cancer diagnosis.

Recently, the photoacoustic imaging has taken advantage of plasmonic systems, such as AuNPs with various sizes and shapes.[69] Plasmon resonances of AuNPs can be tuned to enhance the optical response,[70,71] which can give rise to heat conversion with high efficiency and to the subsequent pressure wave generating the photoacoustic signal. Indeed, these properties have been utilized to develop AuNPs as contrast agents for the photoacoustic imaging.[72] Recently, an amphiphilic GNR coated with PEG and poly(lactic-*co*-glycolic acid) (PLGA; AuNR·PEG·PLGA) was developed for the photoacoustic imaging in xenografted mice.[73] The AuNR·PEG·PLGA could self-assemble into vesicles with the AuNRs embedded in the shell formed by the PLGA and PEG extending into the aqueous environments to stabilize the structure. Furthermore, the in vivo two-dimensional (2D) and three-dimensional (3D) photoacoustic images show that the strong plasmonic coupling of GNRs in the vesicles induced a high photothermal effect and a photoacoustic signal, which may potentially be used for image-guided phototherapy in the future.[73]

In addition, AuNPs have also been utilized as high-quality CT imaging agents due to better X-ray attenuation properties (atomic number $Z=79$; k-edge value =80.7 keV) than that of iodinated CT contrast agents.[74,75] In addition, the conventional small-molecular CT contrast agents are rapidly cleared by the kidney resulting in short imaging times, whereas the gold surface can be modified with biological stabilizing groups (ie, PEG) to improve the pharmacokinetic properties,[76] which is beneficial for cancer imaging. Recently, a folic acid (FA)-targeted gold nanosphere (FA-PEG-PEI-AuNPs) was developed using PEI and PEG as stabilizing ligands.[77] The intravenous injection of FA-PEG-PEI-AuNPs into an overexpressed folate receptor tumor model resulted in significantly higher CT values in the tumor region compared with nontargeted PEG-PEI-AuNPs. In addition to the "enhanced penetration and retention" (EPR)-based passive tumor targeting, the FA-mediated active targeting was also able to significantly enhance the AuNP accumulation in tumor tissues, resulting in enhanced cancer CT imaging.

In addition, AuNPs are also known to enhance the Raman scattering signal of adjacent molecules, and therefore, surface-enhanced Raman spectroscopy (SERS) imaging aided by gold nanomaterials (spheres, rods, cubes, etc.) has also widely been used in the detection of viruses and cancer cells.[78,79]

Functionalized imaging agents for cancer detection

Hybrid dual imaging technologies, including positron emission tomography (PET)/CT, PET/magnetic resonance imaging (MRI), and ultrasound/CT, have recently become available.[80] Cancer diagnosis clearly benefits from these techniques due to multimodality, as a single agent may avoid the administration of multiple doses. However, the choice of imaging modality must be carefully considered since each one has its own advantages and limitations (ie, modalities with high sensitivity may have poor resolution).

AuNPs can be easily functionalized with additional imaging agents, and improvement in AuNP-based imaging systems may allow the observation of tissues not only on its basic anatomic configuration but also on the molecular level.[42,81,82] Moreover, the real-time noninvasive monitoring potentially enables a rapid decision on whether the treatment regimen is effective in a given patient.[40,83]

Recently, Zhao et al[84] have synthesized gold nanospheres doped with ^{199}Au atoms using a one-step procedure for single-photon emission CT (SPECT)/CT imaging in an orthotopic mouse xenograft of triple-negative breast cancer (TNBC). The high-stable radiolabeling ability resulted from the incorporation of ^{199}Au atoms into the crystal lattice of AuNPs. In addition, the ^{199}Au-doped AuNPs were further modified with 1) PEGylation for favorable pharmacokinetics and 2) D-Ala1-peptide T-amide (DAPTA) for targeting C–C chemokine receptor 5 (CCR5, a prognostic biomarker for breast cancer progression).[84] Results demonstrate the suitability of ^{199}Au for SPECT/CT imaging and the potential of ^{199}Au-AuNP-PEG-DAPTA for accurately detecting CCR5 in vivo.

Moreover, He et al[85] have recently synthesized novel AuNPs for magnetic and CT dual-mode imaging in a mouse xenograft of colorectal cancer. Fe_2O_3 was first coated with Au nanoshell (Fe_2O_3/AuNPs), and subsequently the surface of the Fe_2O_3/AuNPs was modified with lectins (sugar-binding proteins specifically bind to the carbohydrate moieties of the glycans on colorectal cancer cells) through bifunctional PEG-N-hydroxysuccinimide ester disulfide linkers (lectin–PEG–Fe_2O_3/AuNPs). The lectin–PEG–Fe_2O_3/AuNPs demonstrated long circulation time, site-specific tumor distribution, and high-quality MRI and CT contrast enhancement effects in tumor tissues, suggesting that the resultant AuNPs are a promising contrast agent for dual-mode MRI/CT colorectal cancer imaging.

Furthermore, selected examples of AuNP-based systemic cancer imaging are provided in Table 1, including the types

Table 1 A summary of studies on the in vivo use of gold nanocomplexes in systemic cancer imaging

Functional ligand	Cancer type	In vivo model	Imaging technique	Comment	Reference
Gold nanospheres					
Stabilizing ligand: PEG and PEI Targeting ligand: FA	Papilloma (KB cells)	S.C. xenograft mouse	CT	The AuNP-PEI was modified with FA-linked PEG, forming FA-targeted PEGylated AuNPs. The resultant targeted AuNPs presented potential role as a nanoprobe for CT imaging of FA receptor-overexpressing xenografted tumor	77
Stabilizing ligand: PEG fluorescent dye	Colon carcinoma (CT26 cells)	S.C. allograft mouse	CT	The signal intensity and nanoprobe accumulation of Au-NPAPF-PEG in the tumor were up to 24 h post i.v. injection, suggesting the role as a promising nanoprobe for in vivo tumor-targeted CT imaging	87
Stabilizing ligands: PEG and glucose Targeting ligand: glucose	Melanoma (SKMEL23 cells)	S.C. xenograft mouse	CT	The AuNP-labeled T cells were injected intravenously to mice-bearing human melanoma xenografts, and whole-body CT imaging allowed examination of the distribution, migration, and kinetics of T cells	88
Stabilizing ligand: PEG	Lung cancer (SPC-A1 cells)	S.C. xenograft mouse	CT	Results suggest that PEGylated AuNPs can be used as a promising contrast agent with enhanced biocompatibility for CT imaging in cancer diagnosis	89
Hybrid formulation: mesoporous silica NPs Emitter: ^{64}Cu	Lung cancer	Urethane-induced lung cancer mouse	PET	^{64}Cu-labeled gold/mesoporous silica hybrid NPs can successfully detect the existence of clinically relevant spontaneous lung tumors in a urethane-induced lung cancer mouse model through PET imaging	90
Stabilizing ligand: PEG Targeting ligand: TAT Emitter: Gd^{3+}	Glioblastoma (U87 cells)	Orthotopic xenograft mouse	MRI	Compared with the Gd^{3+} chelate, TAT-Au NP-Gd conjugates showed a 2.2-fold higher relaxivity and 82-fold enhancement in Gd^{3+} cellular uptake, which allowed for sensitive detection of the cancer cells via MRI	91
Stabilizing ligand: PEG Targeting ligand: RGD Emitter: ^{125}I	Glioblastoma (U87 MG cells)	S.C. xenograft mouse	SPECT/CT	In vivo SPECT/CT imaging results showed that the ^{125}I-labeled RGD–PEG–AuNP probes can target the tumor site as soon as 10 min after injection	92
Stabilizing ligand: PEG Targeting ligand: DAPTA	TNBC (4T1 cells)	Orthotopic allograft mouse	SPECT/CT	The synthesis of AuNPs was doped with ^{199}Au atoms into the crystal lattice of each AuNP, which ensured the highest possible stability for the radiolabel. When conjugated with DAPTA for the CCR5 receptor, the targeted AuNPs resulted in the in vivo sensitive and specific detection	84
Stabilizing ligand: GC MMP sensitive linker: MMP peptide NIR dye: Cy5.5	Colorectal cancer (HT-29 cells)	S.C. xenograft mouse	CT NIR fluorescence imaging	The quenched Cy5.5 was recovered by cleavage of the peptide substrates upon exposure to the active MMPs, which is overexpressed in tumor tissue. As a result, the AuNPs simultaneously provided CT images with high spatial resolution and optical images with high sensitivity	93
Stabilizing ligand: PEG Targeting ligand: FA Emitter: Gd^{3+}	Papilloma (KB cells)	S.C. xenograft mouse	CT MRI	With the modification of PEG and the FA-targeting ligand, the multifunctional AuNPs were able to be used for dual-mode CT/MRI of xenograft tumor models overexpressing FA receptors	94
Photostability enhancer: PB	Colon adenocarcinoma (HT-29 cells)	S.C. xenograft mouse	PAI CT	The AuNPs were coated with PB to form the core/shell Au@PB NPs, which were found to be an excellent photoabsorbing agent for both PTT and PAI. The gold core ensured a remarkable contrast enhancement for CT imaging	95

(*Continued*)

Table 1 (*Continued*)

Functional ligand	Cancer type	In vivo model	Imaging technique	Comment	Reference
Stabilizing ligand: PEG NIR dye: Cy5.5	Squamous carcinoma (SCC7 cells)	S.C. allograft mouse	PAI NIR fluorescence imaging	The resultant AuNPs showed high fluorescence and PAI signals in the tumor over time, which peaked at the 6 h time point (tumor-to-normal tissue ratio of 3.64±0.51 for optical imaging and 2.5±0.27 for PAI)	96
GNRs					
Stabilizing ligand: PEG Targeting ligand: biotin	Squamous carcinoma (SCC7 cells)	S.C. allograft mouse	PAI	Under the photothermal/photoacoustic imaging, the in vivo pharmacodynamic effect of resultant GNRs could be monitored by precisely controlling the irradiation time and intensity of the NIR light	97
Amphiphilic ligands: PEG and PLGA	Glioblastoma (U87 MG cells)	S.C. xenograft mouse	PAI	Amphiphilic AuNRs were prepared by grafting with PEG and PLGA forming vesicles. Enhanced PA signals were due to the strong plasmonic coupling of the gold in the vesicular shell	73
Stabilizing ligand: PEG Targeting ligand: CET	Epithelial carcinoma (A431 cells)	S.C. xenograft mouse	NIR fluorescence imaging	The NIR absorption images showed that the relative total photon counts from targeted Au nanorods in tumor tissue at 6 h were 10-fold higher than those from nontargeted counterparts	68
Stabilizing ligand: PEG NIR dye and photosensitizer: $AlPcS_4$	Squamous carcinoma (SCC7 cells)	S.C. xenograft mouse	NIR fluorescence imaging	After i.v. injection of the AuNP–$AlPcS_4$ complex, tumor sites were clearly identified on NIR fluorescence imaging as early as 1 h after injection	98
Stabilizing ligand: PNIPAAmMA MRI contrast agents: Fe_3O_4 NPs	Glioma (C6 cells)	S.C. xenograft mouse	PET PAI	GNRs were coated with PNIPAAmMA and Fe_3O_4 NPs using a simple LbL method, demonstrating the accurate tumor location using dual MRI and PAI	99
Stabilizing ligand: PEG SERS reporters	Ovarian cancer (MDA-435S, HEY, SKOV3 cells)	S.C. xenograft mouse	PAI SERS imaging	PEGylated Au nanorods allowed presurgical PAI visualization of a tumor for locoregional staging as well as intraoperative SERS imaging for complete resection of tumor margins	100
Stabilizing ligand: liposome	Liver cancer (HepG2, Huh-7)	Orthotopic xenograft mouse	PAI NIR fluorescence imaging	ICG-loaded liposome-Au nanorods exhibit favorable biocompatibility, high stability, and enhanced dual-model imaging signal	101
Gold nanoshells					
Stabilizing ligand: PPAA shell Targeting ligand: CET Emitter: ^{89}Zr	Epithelial carcinoma (A431 cells)	S.C. xenograft mouse	PET	PET studies showed that the resultant AuNPs–PPAA–CET–^{89}Zr provided high tumor-to-background ratio, suggesting a valuable tool for theranostic purposes	102
Stabilizing ligand: PEG Emitter: ^{64}Cu	Head and neck squamous cell carcinoma (SCC4 cells)	S.C. xenograft rat	PET/CT	The in vivo distribution of ^{64}Cu-Au nanoshells was monitored using PET/CT imaging at various time points after i.v. injection	103
Targeting ligand: lectin MRI contrast agents: Fe_3O_4 NPs	Colorectal cancer (SW620 cells)	S.C. xenograft mouse	MRI CT	The lectin–Fe_2O_3@Au nanoshells showed great potential for dual-mode MRI and CT imaging of colorectal cancer in vivo	85
Targeting ligand: antibody (anti-NGAL) MRI contrast agents: Fe_3O_4 NPs	Pancreatic cancer (AsPC-1 cells)	S.C. xenograft mouse	MRI NIR fluorescence imaging	Antibody-conjugated Au nanoshells specifically targeted pancreatic cancer cells in vivo providing contrast for both NIR fluorescence and T2-weighted MRI with high tumor contrast	104
Stabilizing ligand: PEG Emitter: Gd^{3+}	Melanoma (B16-F10 cells)	S.C. xenograft mouse	MRI X-ray imaging Optical imaging	The Gd^{3+}-conjugated Au-silica nanoshells showed great potential for multimode MRI, X-ray imaging, and optical imaging of melanoma in vivo	105

(*Continued*)

Table 1 (*Continued*)

Functional ligand	Cancer type	In vivo model	Imaging technique	Comment	Reference
MMP-triggering ligand: gelatin MRI contrast agent: Fe_3O_4	Hepatoma (H22 cells)	S.C. allograft mouse	CT and PAT imaging and MRI	A bio-eliminable MPNA, assembled from Fe_3O_4 nanocluster and gold nanoshell, could respond to the local microenvironment with acidic pH and enzymes in tumors, collapse into small molecules and discrete NPs, and finally be cleared from the body	106
Gold nanoclusters					
Stabilizing ligand: BSA Targeting ligand: methionine NIR dye: hydrophilic ICG	Breast cancer (MDA-MB-231 cells)	S.C. xenograft mouse	NIR fluorescence imaging	The fluorescence signal in receptor-positive tumor was distinguishable from the normal tissues at 2 h post injection, reached peak intensity at 10 h post injection, and was still detectable at 96 h	107
Stabilizing ligand: BSA Targeting ligand: FA and HA	Liver cancer (HepG2 cells) Adenocarcinoma (A549 cells)	S.C. xenograft mouse	NIR fluorescence imaging	The strong fluorescence was observed at the tumor sites derived from the selectively accumulated targeted AuNPs, demonstrating a promising probe for the cancer diagnosis	108
Stabilizing ligand: BSA Nuclear imaging moiety: Hoechst	Pancreatic tumor (MiaPaca-2 cells)	S.C. xenograft mouse	Maestro™ 2 in vivo imaging system	The in vivo imaging was performed via blue and red channels which displayed the accumulation of Hoechst-AuNCs mainly in the tumor and partly in the liver and kidneys	109
Stabilizing ligand: PEG Emitter: ^{64}Cu	Prostate cancer (PC3 cells)	S.C. xenograft mouse	PET/CT	PET/CT results demonstrated the heterogeneous intratumoral distribution of $^{64}CuAuNCs$-PEG350 and $^{64}CuAuNCs$-PEG1000	110
Emitter: ^{64}Cu	Glioblastoma (U87 MG cells)	S.C. xenograft mouse	PET IVIS® imaging system	^{64}Cu-dopped AuNCs showed satisfactory synergistic dual-modality PET and self-illuminating NIR tumor imaging	111
Stabilizing ligand: BSA Emitter: Gd^{3+}	Breast cancer (MCF-7 cells)	S.C. xenograft mouse	CT NIR fluorescence imaging MRI	The hybrid gold–gadolinium nanoclusters provided a promising nanoprobe for cancer-targeted imaging and diagnosis in vivo	112
Stabilizing ligand: hairpin-DNA	Melanoma (M14 cells)	S.C. xenograft mouse	NIR fluorescence imaging	The hairpin-DNA-modified $NaYF_4@SiO_4$-Au promoted simultaneous deep tissue imaging and drug molecule release when combining single-band anti-stokes NIR emission and the photothermal effect	113
pH-sensitive ligand: azide and alkyne functionalities	Glioma (U87MG cells)	Orthotopic xenograft mouse	MRI and SERS imaging	Multifunctional AuNPs could not only preoperatively define orthotopic glioblastoma xenografts by MRI with high sensitivity and durability in vivo but also intraoperatively guide tumor excision with the assistance of a handheld Raman scanner	114
Hollow AuNPs					
Stabilizing ligand: PEG	Adenocarcinoma (A549 cells)	S.C. xenograft mouse	CT	The attenuation coefficient of hollow AuNPs is 5.3 times higher than that of the iodine-based contrast agent at the same concentration, demonstrating the potential of hollow AuNPs for CT imaging	115
Stabilizing ligand: PEG Targeting ligand: RGD Emitter: ^{64}Cu	Liver carcinoma VX2 tumor)	Orthotopic allograft rabbit	PET/CT	PET/CT images showed that the ^{64}Cu-RGD-PEG-HAuNS showed higher tumor uptake than control groups at 24 h post injection	116
Stabilizing ligand: PEG Targeting ligand: RGD Emitter: ^{64}Cu	Glioblastoma (U87 cells)	Orthotopic xenograft mouse	PET/CT PAI	The dual-modality PAI and PET/CT imaging provided a promising targeted AuNP-mediated glioma therapy	117
Gold nanostars					
Stabilizing ligand: PEG Raman reporter: p-mercaptobenzoic acid	Primary soft-tissue sarcomas	Transgenic mouse	CT Two-photon luminescence imaging	The CT and optical results showed that 30 nm nanostars have higher tumor uptake, as well as deeper penetration into tumor interstitial space compared with 60 nm counterparts	118

(*Continued*)

Table 1 (*Continued*)

Functional ligand	Cancer type	In vivo model	Imaging technique	Comment	Reference
Stabilizing ligand: PEG	Breast cancer (4T1 cells)	S.C. allograft mouse	PAI	Novel Fe_2O_3@Au core/shell magnetic gold nanoflowers were synthesized through interactive growth of Au on Fe_2O_3 NPs. The nanoflowers exhibited remarkable SERS enhancement	119
Emitter: Gd^{3+}	Adenocarcinoma (A549 cells)	S.C. xenograft mouse	MRI, CT, and NIR fluorescence imaging	The existence of Gd^{3+} ions on GNCNs exhibits significant luminescence intensity enhancement for NIR fluorescence imaging, high X-ray attenuation for CT imaging, and reasonable r1 relaxivity for MRI	120
SERS labeling ligand: DTNB	Ovarian cancer (SKOV3)	S.C. xenograft mouse	Raman spectroscopy	The SERS Au nanostars were developed as a highly sensitive contrast agent for tumor detection in xenografted mice	121
Gold nanocages					
Stabilizing ligand: PEG Emitter: ^{64}Cu	Breast cancer (EMT-6 cells)	S.C. xenograft mouse	PET/CT	PET/CT images clearly showed rapid localization of the ^{64}Cu -PEG-Au nanocages in tumor at 1 h post injection with the administration of a trace amount	122
Gold nanoprisms					
Stabilizing ligand: PEG	Colorectal cancer (HT-29 cells)	S.C. xenograft mouse	PAI	PEGylated Au nanoprisms showed the capacity to penetrate tumors and provided a high-resolution signal amplifier for optoacoustic imaging	123
Gold nanotripods					
Stabilizing ligand: PEG Targeting ligand: RGD	Glioblastoma (U87 MG cells)	S.C. xenograft mouse	PAI	i.v. injection of RGD-conjugated Au-tripods showed PAI contrasts in tumors up to threefold higher than for the blocking group (coinjection with RGD)	124

Abbreviations: AIE, aggregation-induced emission; AuNPs, gold NPs; BSA, bovine serum albumin; CET, cetuximab; CT, computed tomography; DAPTA, D-Ala1-peptide T-amide; DTNB, 5,5-dithio-bis-(2-nitrobenzoic acid); FA, folic acid; GC, glycol chitosan; GNRs, gold nanorods; HA, hyaluronic acid; ICG, indocyanine green; i.v., intravenous; LbL, layer-by-layer; MMP, matrix metalloproteinase; MPNA, magnetoplasmonic nanoassembly; MRI, magnetic resonance imaging; NGAL, neutrophil gelatinase-associated lipocalin; NIR, near-infrared; NPs, nanoparticles; PAI, photoacoustic imaging; PB, Prussian blue; PEG, polyethylene glycol; PEI, polyethylenimine; PET, positron emission tomography; PLGA, poly(lactic-*co*-glycolic acid); PPAA, plasma-polymerized allylamine shell; PTT, photothermal therapy; SPECT, single-photon emission CT; S.C., subcutaneous; SERS, surface-enhanced Raman spectroscopy; TAT, transactivator of transcription; TNBC, triple-negative breast cancer.

of AuNPs, functional ligands, cancer types, in vivo animal models, imaging techniques, and end point comments.

AuNPs for cancer phototherapy

PTT

In addition to the aforementioned enhanced light scattering (referred as a radiative property) useful for optical imaging, AuNPs can also convert the absorbed light into heat via a series of nonradiative processes.[86,125–129] Two main processes occur based on the heat energy contents: 1) the heat from the energy transformation is passed to the surrounding medium via the phonon–phonon relaxation within ~100 ps and 2) a competitive process takes place between the heating by the electrons and the cooling by the surrounding medium, and when the heating rate is much faster than the cooling rate, AuNPs are melted in hundreds of femtoseconds.[125–128] To facilitate cancer PTT, the first process has to dominate, and therefore, continuous-wave (CW) lasers that overlap maximally with the AuNP SPR absorption band need to be utilized.[130,131]

PTT can be achieved using gold nanospheres under the stimulation of pulsed or CW visible lasers due to the SPR absorption in the visible region, whereby such treatment is suitable for shallow tumors (ie, skin cancer).[132,133] Recently, antibody-targeted gold nanospheres were developed to specifically target the EGFR on squalors carcinoma cells, and following stimulation by single 10 ns laser pulses at visible wavelengths, the resultant AuNPs generated intracellular photothermal micro bubbles and induced PTT for tumor inhibition in a subcutaneous cancer model.[134]

To treat tumors under the skin, NIR-active PTT is favorable as the light can penetrate more deeply due to the minimal absorption of the hemoglobin and water in tissues in this spectral region. Therefore, it is important to tune the SPR absorption of AuNPs to the NIR region by means of altering the shape, morphology, and structure, as described in the "Optical characteristics of AuNPs" section.

Recently, RGD-conjugated dendrite-modified GNRs (RGD-diners) were developed by Li et al[135] for selective

tumor targeting and PTT in xenografted mice. At 6 h after intravenous injection, the resultant AuNPs accumulated inside tumor tissues via targeting the $\alpha_v\beta_3$ overexpressed on cancer cells, and when it was irradiated with a NIR laser with a wavelength of 808 nm at a power density of 24 W/cm^2 (~0.5 cm diameter illuminated region), tumor growth was significantly reduced by RGD-diners in comparison with the control groups.

In addition, polymeric per fluorocarbon Nan capsules were prepared using the oil-in-water emulsion method, followed by the addition of PEGylated gold nanoshells on the surface.[136] These resultant Nan capsules could not only enhance the contrast for ultrasound/CT imaging but also function as photo-absorbers for NIR-active PTT in xenografted mice.[136]

Recently, Ayala-Orozco et al[137] have developed novel gold nanomatryoshkas composed of concentric gold–silica–gold layers and PEG-stabilizing ligands, for PTT of TNBC. In comparison with ~150 nm conventional silica–Au nanoshells, the resultant gold nanomatryoshkas (<100 nm) facilitated higher accumulation in tumors due to better penetration of smaller AuNPs into tissue via the EPR effect. Under irradiation with a CW laser emitting 3 W/cm^2 at a wavelength of 808 nm (~1.2 cm diameter illuminated region), the survival rate of an advanced TNBC model with >1,000 mm^3 tumors was significantly improved by gold nanomatryoshkas relative to conventional silica–Au nanoshells.[137]

Photodynamic therapy (PDT)

When photosensitizers are stimulated under the light of specific wavelengths, they convert the surrounding oxygen into toxic reactive oxygen species (ie, singlet oxygen) that may destroy malignant cells in surrounding proximity, which is now known as cancer PDT.[138] However, most of the organic photosensitizers are only activated by UV and visible lights, which have poor tissue penetration and therefore are limited to the treatment of surface tumors.[139] In addition, organic photosensitizers possess low molar extinction coefficients and therefore can undergo photobleaching and enzymatic degradation.[139] In contrast, metal nanostructures (ie, gold, silver, and platinum) can overcome these limitations, as they possess 5–6 orders of molar extinction coefficients, better photostability, and enhanced resistant to enzymatic degradation.[140]

To tackle the treatment of deeply buried tumors, AuNPs that are able to exert PDT upon NIR light activation have recently been developed. For example, lipid-coated gold nanocages were produced to activate PTT and PDT simultaneously in melanoma-xenografted mice.[141] Following direct injection of lipid-coated gold nanocages into the tumor site, a 980 nm CW laser (150 mW/cm^2; 10 min) was used to stimulate AuNPs, which raised temperature (~10°C) and generated the singlet oxygen. As a result, this treatment significantly inhibited tumor growth in comparison with an irradiation of the 808 nm diode laser (150 mW/cm^2; 12 min; only PTT was induced in this wavelength).

In addition, a variety of organic photosensitizers with NIR-active property can also be incorporated into AuNPs for PDT with a low dose of organic photosensitizers and short exposure of laser irradiation. For example, indocyanine green (ICG, a medical diagnostic agent) is used to produce singlet oxygen for PDT.[142] Recently, GNR/ICG-loaded chitosan nanospheres (CS-AuNR-ICG NSs) were prepared by the non-solvent counterion complexation method and electrostatic interaction.[142] The CS-AuNR-ICG NSs could effectively load ICG and protect it from rapid hydrolysis. Results of in vivo NIR fluorescence imaging and biodistribution showed that these Au-chitosan NPs could be specifically delivered to the tumor site. Under an 808 nm laser, CS-AuNR-ICG NSs simultaneously produced hyperthermia and reactive oxygen species, which achieved complete inhibition of tumor growth in xenografted mice. Compared with PTT (GNRs) or PDT (ICG) alone, the combined therapy showed a significantly improved therapeutic efficacy.[142]

In addition, selected examples of AuNP-based cancer phototherapy are provided in Table 2, including the types of AuNPs, functional ligands, cancer types, in vivo animal models, laser types, and end point comments.

Barriers to the translation of AuNPs for cancer theranostics

Although local administration of therapeutics has demonstrated significant potential for the treatment of shallow cancers (ie, skin cancer and head and neck cancer) due to the ease of access, many diseases (eg, metastatic cancers) still require systemic administration of therapeutic agents into the bloodstream. In this section, major challenges, namely, 1) instability in the blood circulation, 2) targeting to specific cells of interest, and 3) activation in response to the tumor microenvironment (TME),[174] for systemic AuNP delivery in terms of cancer diagnosis and phototherapeutics are discussed (Figure 2).

Blood circulation

It has been reported, following intravenous administration, that rapid glomerular filtration occurs in the case

Table 2 A summary of studies on the in vivo use of gold nanocomplexes in systemic cancer PTT and PDT

AuNP type	Functional ligand	Cancer type	In vivo model	Laser	Comment	Reference
PTT						
Au nanorods	Stabilizing ligand: PEG	Melanoma (MDA-MB-435 cells)	S.C. xenograft mouse	810 nm laser 2 W/cm^2 5 min	A single i.v. injection of PEG-Au nanorods enabled destruction of the irradiated human xenograft tumors in mice	143
Au nanorods	Stabilizing ligand: PEG Targeting ligand: RGD	Glioblastoma (U87 MG cells)	S.C. xenograft mouse	808 nm laser 1 W/cm^2 10 min	Au nanorods showed high tumor-targeting ability via receptor-mediated pathway and were successfully used for PTT	144
Au nanorods	Coating material: silica	Breast cancer (4T1 cells)	S.C. allograft mouse	808 nm laser 4 W/cm^2 10 min	When Au nanorods were stimulated with the NIR laser, DOX was released for synergistic therapeutic effect in combination with PTT	145
Au nanorods	Stabilizing ligand: PEG and dendrimers	Colon carcinoma (26 cells)	S.C. allograft mouse	808 nm laser 0.24 W/cm^2 10 min	The combined photothermal-chemo treatment using AuNPs containing DOX for synergistic PPT and chemotherapy exhibited higher therapeutic efficacy than either single treatment alone	146
Au nanorods	Coating materials: PVP and $AgNO_3$ Targeting ligand: aptamer	Adenocarcinoma (A549 cells)	S.C. xenograft mouse	980 nm laser 0.84 W/cm^2 5 min	The resultant AuNPs specifically accumulated into tumor tissues and induced PTT for dramatically stronger antitumor effect upon NIR laser irradiation	147
Au nanorods	Au nanorods encapsulated in CHI/sodium ALG microcapsules	Breast cancer (4T1 cells)	S.C. allograft mouse	808 nm laser 3.83 J/cm^2 5 min	Self-assembled Au nanorods in bilayer-modified microcapsules localized at tumor sites, generated vapor bubbles under NIR exposure, and subsequently damaged tumor tissues	148
Au nanorods	Stabilizing ligand: PEG Targeting ligand: antibody for anaerobic bacteria (*C. difficile*)	Adenocarcinoma (A549 cells)	S.C. xenograft mouse	808 nm laser 0.5 W/cm^2 10 min	The *C. difficile* spores was i.v. injected for 2 days, followed by the injection of antibody-Au nanorods to specifically target the germination of the *C. difficile* spores in tumor tissues (low level of oxygen microenvironment). Under the NIR laser, antibody-Au nanorods completely inhibited tumor growth	149
Au nanorods	Stabilizing ligand: dendrimer	Non-small-cell lung cancer (PC-9 cells)	S.C. xenograft mouse	808 nm laser 3.6 W/cm^2 8 min	Dendrimer-stabilized Au nanorods (DSAuNRs, sub-10 nm in length) showed significantly enhanced absorption in the NIR region compared with dendrimer-stabilized Au nanospheres. The tumor growth was significantly retarded by the photothermal efficiency of DSAuNRs	150
Au nanorods	Coating material: silica Targeting ligand: antibody for CXCR4	Gastric cancer (MGC803 cells)	S.C. xenograft mouse	808 nm laser 1.5 W/cm^2 3 min	iPS cells were transfected with the resulted AuNRs@SiO2@CXCR4 via receptor-mediated pathway. The transfected iPS cells were homing to tumor tissues, and the tumor growth was significantly slowed down by the photothermal efficiency of AuNRs@SiO2@CXCR4	151
Au nanoshells	Multilayered AuNPs with silica and gold, also termed Au nanomatryoshkas	Breast cancer (MDA-MB-231 cells)	Orthotopic xenograft mouse	810 nm laser 2 W/cm^2 5 min	Au nanomatryoshkas exhibited improved PTT efficacy when compared with conventional gold nanoshells	152
Au nanoshells	Stabilizing ligand: PEG	Breast cancer (4T1 cells)	S.C. allograft mouse	808 nm laser 1 W/cm^2 10 min	In combination with chemotherapeutics, the resultant Au nanoshells achieved complete destruction of the tumors at a low laser irradiation without weight loss or recurrence of tumors	153

(*Continued*)

Table 2 (*Continued*)

AuNP type	Functional ligand	Cancer type	In vivo model	Laser	Comment	Reference
Au nanoshells	Stabilizing ligand: PEG Inner core: PLGA NPs	Glioblastoma (U87 MG cells)	S.C. xenograft mouse	808 nm laser 1.5 W/cm^2 1.5 min	The temperature of tumor treated with the resultant Au nanoshells was rapidly increased to 46.6°C, which released DOX for synergistic therapeutic effect in combination with PTT	154
Au nanoshells	Stabilizing ligand: PEG Inner core: PEI-PAsp (DIP/MEA) NPs	Liver cancer Bel-7402 cells	S.C. xenograft mouse	808 nm laser 1.5 W/cm^2 2 min	A polymeric vesicle encapsulating DOX was prepared and then decorated with a gold layer using a modified method of in situ gold seed growth. The NIR light energy was converted into heat, which killed cancer cells in the vicinity and induced the rupture of nanoshell to release DOX inside tumor	155
Au nanoshells	Stabilizing coating: MPCMs Inner core: silica	Breast cancer (4T1 cells)	S.C. allograft mouse	808 nm laser 1 W/cm^2 5 min	MPCM-coated Au nanoshells presented longer blood circulation and tumor accumulation in a xenograft mouse model of breast cancer. Tumor growth was significantly slowed down by irradiation of NIR laser	156
Au nanostars	Stabilizing ligand: PEG Targeting ligand: RGD	Glioblastoma (U87 MG cells)	S.C. xenograft mouse	790 nm laser 1 W/cm^2 10 min	RGD-Au nanostars were designed to specifically target overexpressed integrin $\alpha_v\beta_3$ on tumor neovasculature, enabling highly sensitive PTT	157
Au nanostars	Surface coating: organosilica	Breast cancer (MDA-MB-231 cells)	S.C. xenograft mouse	808 nm laser 0.5 W/cm^2 5 min	In 5 min of irradiation, the temperature at the tumor region of mice treated with Au nanostars increased remarkably to about 57°C	158
Au nanocages	Targeting ligand: HA	Breast cancer (MDA-MB-231 cells)	S.C. xenograft mouse	808 nm laser 1 W/cm^2 5 min	HA-coated Au nanocages accumulated inside tumor tissues via HA-CD44 interaction. Under the NIR stimulation, HA-coated Au nanocages significantly slowed down the tumor growth. In addition, a complete tumor inhibition was achieved when combined with chemotherapy	159
Au nanocages	Gold surface was coated with PVP and RBC membranes	Breast cancer (4T1 cells)	S.C. allograft mouse	850 nm laser 1 W/cm^2 10 min	RBC-AuNCs exhibited significantly enhanced in vivo blood retention and circulation lifetime. With NIR laser, RBC-AuNCs achieved 100% survival of tumor-bearing mice over a span of 45 days	160
Hollow Au nanospheres	Stabilizing ligand: PEG Targeting ligand: a peptide (TNYL)	Ovarian carcinoma (SKOV3 cells)	S.C. xenograft mouse	808 nm laser 1.5 W/cm^2 3 min	Under NIR laser irradiation, the resultant hollow Au nanospheres induced PTT for dramatically stronger antitumor effect against EphB4-positive tumors than EphB4-negative tumors	161
Hollow Au nanospheres	Stabilizing ligand: PVP and citrate	Ovarian carcinoma (SKOV3 cells)	S.C. xenograft mouse	808 nm 3.0 W/cm^2 10 min	The resultant AuNPs exhibited a significantly enhanced surface plasmon absorption in the NIR region, inducing an efficient photothermal conversion and stronger anticancer ability under NIR laser irradiation	162
Au nanoclusters	A pH-sensitive ligand inducing Au nanoclusters in mild acidic environments	Fibrosarcoma (HT-1080 cells)	S.C. xenograft mouse	660 nm laser 0.5 W/cm^2 1 min	MSCs were first transfected with the resultant AuNPs. The MSC-AuNPs showed a 37-fold higher tumor-targeting efficiency and resulted in a significantly enhanced anticancer effect upon irradiation	163

(*Continued*)

Table 2 (*Continued*)

AuNP type	Functional ligand	Cancer type	In vivo model	Laser	Comment	Reference
Au nanoplates	Stabilizing ligand: PEG	Breast cancer (4T1 cells)	S.C. allograft mouse	808 nm laser 0.5 W/cm^2 10 min	PEGylated AuNPs presented good biocompatibility, prolonged blood circulation, and relatively high tumor accumulation. The NIR laser irradiation induced PTT and retarded tumor growth	164
PDT						
Au nanospheres	Coating materials: heparin Photosensitizer: PhA	Adenocarcinoma (A549 cells)	S.C. xenograft mouse	670 nm laser 3 mW/cm^2 30 min	The PDT effects of PhA-H/AuNP significantly retarded tumor growth in comparison with PhA alone	165
Au nanorods	Coating materials: silica and PEG Photosensitizer: PPIX	Adenocarcinoma (HeLa cells)	S.C. xenograft mouse	532 nm laser 25 mW/cm^2 15 min	A real-time and specific in vivo SERS and fluorescence detection method using the resultant AuNPs was applied for tumor detection and subsequent PDT	166
Au nanorods	AuNPs encapsulated in Pluronic nanogel Photosensitizer: Ce6	Squamous carcinoma (SCC7 cells)	S.C. allograft mouse	655 nm laser 20 J/cm^2 30 min	A remarkable synergy for anticancer treatment was observed when PDT was applied before PTT, both in vitro and in vivo	167
Au nanorods	Stabilizing ligand: PEG Targeting ligand: FA	Melanoma (B16F0 cells)	S.C. allograft mouse	915 nm 130 mW/cm^2 15 min	GNRs alone can sensitize the formation of singlet oxygen and exert dramatic PDT effects on complete destruction of tumors in mice under light excitation	168
Au nanorods	Stabilizing ligand: CHI Photosensitizer: ICG	Liver cancer (H22 cells)	S.C. allograft mouse	808 nm laser 2 W/cm^2 10 min	The resultant NPs have been successfully prepared to facilitate in vivo PDT resulting in abundant ROS produced by ICG under NIR irradiation	142
Au nanorods	Stabilizing ligand: poly(allylamine hydrochloride) Photosensitizer: RB	Oral squamous carcinoma	A carcinogen was topically injected into the left cheek pouch mucosa	532 nm green light 1.79 W/cm^2 10 min	The PDT-only treatment achieved a 46.5% tumor inhibition rate; when combined with PTT effects under NIR laser stimulation, 95.5% tumor inhibition rate was achieved	169
Au nanorods	Endosome disruptive ligand: Tat/HA2 Photosensitizer: $AlPcS_4$	Adenocarcinoma (HeLa cells)	S.C. xenograft mouse	808 nm laser 400 mW/cm^2 15 min and 680 nm LED light 10 mW/cm^2 40 min	AuNRs absorbed an SPR wavelength (808 nm) and converted it into heat, causing the release of $AlPcS_4$. Subsequently, upon illumination at 680 nm, the released $AlPcS_4$ transferred the photon energy to oxygen molecules, stimulating ROS generation to slow down the tumor growth	170
Au nanocages	Stabilizing ligand: PEG Photosensitizer: HPPH	Colon cancer (Colon-26 cells)	S.C. allograft mouse	665 nm laser 75 mW/cm^2 30 min	The tumor growth was suppressed due to the enhanced phototoxicity of the HPPH-Au nanocages under the laser stimulation	171
Au nanoclusters	AuNPs encapsulated in silica Photosensitizer: Ce6	Melanoma (MDA-MB-435 cells)	S.C. xenograft mouse	671 nm laser 100 mW/cm^2 10 min	The resultant AuNCs@SiO_2–Ce6 completely inhibited tumor growth in mice due to PDT effects when compared with Ce6 alone and AuNCs@SiO_2 alone	172
Au quantum clusters	Stabilizing ligand: lipoic acid Targeting ligand: FA Photosensitizer: PPIX	Glioma (C6 cells)	S.C. xenograft mouse	532 nm laser 1.5 W/cm^2 15 min	Under the laser stimulation, singlet oxygen efficiency of the resultant NPs was significantly higher when compared with that of the PPIX alone	173

Abbreviations: ALG, alginate; AuNPs, gold NPs; *C. difficile*, *Clostridium difficile*; Ce6, chlorin e6; CHI, chitosan; DOX, doxorubicin; FA, folic acid; GNRs, gold nanorods; HA, hyaluronic acid; HPPH, 3-devinyl-3-(1′-hexyloxyethyl)pyropheophorbide; ICG, indocyanine green; iPS, Induced pluripotent stem; i.v., intravenous; LED, light-emitting diode; MPCMs, macrophage cell membranes; MSCs, mesenchymal stem cells; NIR, near-infrared; NPs, nanoparticles; PDT, photodynamic therapy; PEG, polyethylene glycol; PEI, polyethylenimine; PEI-PAsp (DIP/MEA), polyethylenimine-b-poly(2-diisopropylamino/2-mercaptoethylamine) ethyl aspartate; PhA, pheophorbide a; PLGA, poly(lactic-*co*-glycolic acid); PPIX, protoporphyrin IX; PTT, photothermal therapy; PVP, polyvinylpyrrolidone; RB, Rose Bengal; RBC, red blood cell; ROS, reactive oxygen species; S.C., subcutaneous; SERS, surface-enhanced Raman spectroscopy; SPR, surface plasmon resonance.

of NPs with a hydrodynamic size of <6 nm, while those with particle sizes of >8 nm are able to avoid kidney removal.[175] While NPs with >10 nm diameter may reduce renal filtration, larger particles (ie, >100 nm) can evoke the reticuloendothelial system (RES).[176] The RES, also known as the mononuclear phagocyte system (MPS), is part of the immune system, which primarily involves the liver, spleen, and lymph nodes.[176,177] Foreign materials will be removed

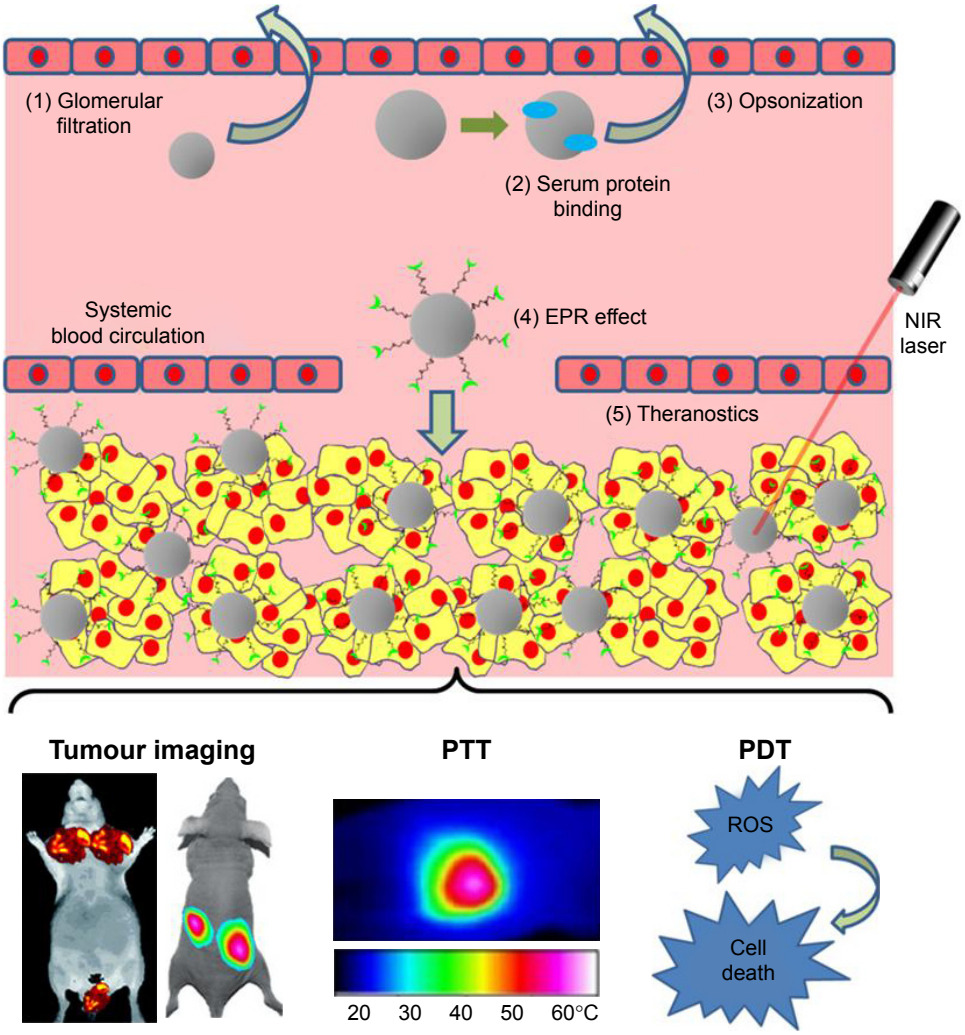

Figure 2 Systemic delivery of multifunctional AuNPs for cancer bioimaging and phototherapeutics.
Notes: (1) Following intravenous injection into the blood, AuNPs with a particle size of <6 nm are prone to glomerular filtration. (2 and 3) When blood proteins bind to AuNPs nonspecifically, the resultant complexes tend to be taken up by MPS for opsonization (a means of identifying the invading particle to the phagocyte). (4) Multifunctional AuNPs (~100 nm) with stealth coating materials, bioresponsive moieties, bioactive targeting ligands, and/or bioimaging agents can efficiently accumulate inside tumor tissues via the "EPR" effect and specifically target cancer cells via ligand–receptor pathway. (5) As a result, theranostic AuNPs can sensitively image the tumors and effectively induce PTT and/or PDT under the irradiation of the NIR light.
Abbreviations: AuNPs, gold nanoparticles; EPR, enhanced penetration and retention; MPS, mononuclear phagocyte system; NIR, near-infrared; PDT, photodynamic therapy; PTT, photothermal therapy; ROS, reactive oxygen species.

out of the blood circulation by the immune cells in MPS, thus dramatically reducing the circulatory half-time ($t_{1/2}$) of NPs.[177] In addition, nonspecific adsorption of blood proteins onto the surface of NPs (ie, hydrophobic interactions between hydrophobic patches on proteins and hydrophobic ligands on NPs, and electrostatic interactions between anionic albumin and cationic NPs) may inhibit NPs' targeting capabilities or increase the overall particle size of NPs, and eventually the resultant large complexes are either trapped in the capillary endothelium of the lung or taken up by MPS.[176]

The modification of stabilizing ligands (ie, PEG, block copolymers, and hyaluronic acid [HA]) onto the gold surface, forming the so-called "stealth" particles capable of improving pharmacokinetic profiles, has been substantially reviewed previously.[76,178,179] In addition to these stabilizing components, long-circulating NPs have also been developed where the NP surface is coated with the cellular membrane of red blood cells (RBCs) and leukocytes.[150,154,174,175] As an alternative stealth coating material, the membrane of these cells completely covers the NP surface with their "self-markers" (ie, proteins, glycans, and acidic sialyl moieties), and the resultant NPs, recognized as the host's own cells, can actively evade the immune system. For example, Piao et al[160] reported that the RBC-coated gold nanocages exhibited longer blood retention compared with the PEGylated counterparts. In addition, the fusion of RBC membranes over gold surface did not alter the unique porous and hollow structures of gold nanocages. Following systemic administration, the

RBC-coated gold nanocages demonstrated enhanced tumor accumulation, induced NIR-active PTT, and eventually achieved 100% survival of tumor-bearing mice over a span of 45 days.[160]

Targeting to specific cells of interest

It is known that tumor grows rapidly via a process termed angiogenesis (new blood vessels are developed from the preexisting vasculature).[177,180] The porous vasculature of a tumor is known to provide access to blood-circulating particles with sizes <500 nm, usually <150 nm.[176] In addition, the lymphatic drainage system of tumor tissues is normally underdeveloped, and thus, NPs may not be removed. This EPR effect will facilitate "passive" accumulation of NPs in tumor tissues. In addition, targeting ligands (ie, antibodies and peptides) can be functionalized on NPs for "active" cancer targeting. Taking advantage of the "passive" and "active" targeting, recent advances in the design of AuNPs have offered great potential for accurate diagnosis and targeted therapy. For example, targeted gold nanocages were developed by coating with HA (a targeting ligand for CD44) on the gold surface to specifically recognize cancer cells overexpressing CD44.[159] The HA–Au nanocages containing DOX could be efficiently uptaken by a receptor-mediated process, and subsequently, the coated HA molecules were degraded in lysosomes, resulting in the release of DOX. Biodistribution results demonstrate that targeted gold nanocages achieved significantly higher tumor accumulation relative to nontargeted counterparts in tumor-bearing mice. As a result, HA-coated gold nanocages containing DOX significantly slowed down the tumor growth, and more importantly, complete tumor inhibition was achieved when combined with PTT under the NIR stimulation.[159]

Activation in response to TME

TME is specifically adapted to support the growth, invasion, and metastasis of primary tumor tissues; this has been substantially reviewed previously.[181] "Smart" bioresponsive NPs have been developed for targeted delivery and controlled drug release by exploiting the TME, where a slightly acidic environment, a low oxygen (hypoxia) niche, and overexpression of extracellular matrix (ECM) components (ie, MMPs) are evident.[181]

It is now known that the hypoxia region in solid tumors is a complex microenvironment with a low oxygen concentration and deficient nutrients.[182] The hypoxic environment can not only lower the susceptibility of cancer cells to anticancer drugs but also reduce the response of cancer cells to free radicals.[182] Although the hypoxia of solid tumors causes a hurdle in therapy, the low level of oxygen microenvironment serves as an ideal habitat for a number of anaerobic bacteria. Recently, Luo et al[149] reported a tumor-targeted AuNP delivery using two anaerobic bacterial strains, namely, *Bifidobacterium breve* UCC2003 and *Clostridium difficile* CCUG 37780. In this study, two approaches were designed for the active NP delivery: 1) a direct conjugation of GNRs on the surface of the vegetative *B. breve* for intravenous delivery into hypoxic region (a cargo-carrying approach) and 2) the injection of the *C. difficile* spores first, followed by the intravenous administration of the antibody–GNR conjugates to specifically target the germination of the *C. difficile* spores (an antibody-guiding approach). Under NIR excitation, the antibody-directed strategy showed stronger imaging and achieved effective PTT to completely inhibit tumor growth in a subcutaneous mouse cancer model.[149]

In addition, Sun et al[93] developed novel AuNPs for dual CT/optical imaging of cancer. First, AuNPs were modified with glycol chitosan (GC) polymers (GC-AuNPs) for excellent stability and enhanced EPR effect. Second, fluorescent probes were chemically modified to GC-AuNPs via MMP-active peptides (MMP-GC-AuNPs). The NIR fluorescent probes were strongly quenched by the combinational quenching effects between the organic black hole quencher and the gold surface, but the quenched probes were reactivated upon exposure to MPPs in the TME. As a result, CT images with high spatial resolution and optical images with high sensitivity were simultaneously achieved using these AuNP-based CT/optical dual imaging probes.[93]

Biodistribution, metabolism, and nanotoxicity

In addition to tumor accumulation via the EPR effect, a majority of intravenously administrated NPs are nonspecifically distributed into healthy tissues (ie, phagocytic cell-rich organs such as the liver and spleen) before the renal clearance.[183] Although the gold core is generally inert, nontoxic, and biocompatible, significant toxicity of AuNPs can be induced by the synthesis method of gold nanostructures, physicochemical properties (ie, size, morphology, and surface charge), surface conjugates and ligands, the doses, and the administration routes.[173] Recently, numerous studies have described AuNPs designed to investigate whether their in vivo behaviors such as accumulation in healthy tissues and renal clearance cause unwanted effects.[184–187]

For example, the glomerular filtration, biodistribution, and toxicity of glutathione (GSH)- and bovine serum albumin

(BSA)-capped AuNPs were evaluated using mice.[188] As a result, smaller AuNPs (GSH-coated, ~2 nm) caused highly efficient kidney removal and were more readily metabolized relative to the larger AuNPs (BSA-coated, ~8 nm), suggesting that the toxicity was related to the size of AuNPs. In addition, although both AuNPs caused acute infection, inflammation, and kidney function damage after 24 h, these effects were eliminated for ~2 nm AuNPs after 28 days; in contrast, ~8 nm AuNPs further accumulated in the liver and spleen causing irreparable toxicity.[188]

It has been difficult to substantially evaluate the biodistribution, clearance, and toxicity of AuNPs, due to the fact that experimental designs are diverse, including the particle size, charge and shape, functionalization methods, types of animal models, delivery doses, and administration routes. Therefore, standard approaches are urgently needed in the future to facilitate development and approval of AuNPs for cancer theranostics.[189]

Conclusion and future perspectives

The newly emerging concept termed theranostics is well established as the development of novel strategies to combine diagnostic and therapeutic capabilities into a single agent facilitating specific and personalized therapies for diseases.[190] The rationale behind the concept is that diseases, such as cancers, are extremely heterogeneous, and all existing treatments are effective for only certain patients and at selective stages of disease development.[191] Therefore, a combined approach of diagnostics and therapeutics may provide promising treatment protocols that are more specific to individuals, ie, personalized medicines, and therefore more likely to offer improved prognoses.

Recent advances in understanding the optical and chemical properties of gold have enabled the design of novel AuNPs containing diagnostic and therapeutic functions that can be integrated into one system.[40,42,192] Au-nanocomplex-based cancer imaging and phototherapy are reviewed in the "AuNPs for cancer diagnosis" and "AuNPs for cancer phototherapy" sections, respectively (Tables 1 and 2); many of these Au nanocomplexes, by tuning the size, shape, and structure, and by using different functional ligands, are capable of improving sensitive cancer diagnosis and targeted phototherapy simultaneously, under the stimulation of the appropriate light resources (NIR light is preferred in most cases). In addition, a number of AuNP-based theranostics have advanced into clinical trials (NCT03020017, NCT01270139 NCT02755870, NCT01420588, and NCT02782026). For example, the safety evaluation of a drug named NU-0129 is now undertaking an early Phase I trial (NCT03020017). NU-0129 is composed of siRNA arranged on the surface of Au nanospheres, and when infused in patients with recurrent glioblastoma multiforme or gliosarcoma, the Au nanocomplexes can penetrate the blood–brain barrier and deliver siRNA into tumor cells knocking down the expression of oncoprotein Bcl2Like12, which may result in significant inhibition of tumor growth (NCT03020017). Furthermore, CNM-Au8 (a drug candidate now being tested in clinical trial), an Au nanocrystal suspension drug, has recently been developed by Clene Nanomedicine (Salt Lake City, UT, USA) using Clean-Surface Nanosuspension™ (CSN) technology (it produces atomically clean-surface elemental nanocrystals, free of any residual surface chemicals, or surface-capping agents) (www.clene.com). The oral administration of CNM-Au8 has demonstrated efficient immunomodulation in established demyelination animal models (www.clene.com). The safety, tolerability, and pharmacokinetics of CNM-Au8 are now under evaluation in healthy volunteers, with a hope of facilitating the application of the drug for the demyelinating disorder neuromyelitis optica (NMO) in the future (NCT02755870).

To overcome in vivo delivery barriers, Au nanocomplexes are normally modified with functional moieties such as stabilizing materials, targeting ligands, and bioresponsive linkers. However, it should be borne in mind that extensive functional modifications may cause unwanted toxic side effects, and therefore, further investigation is required to quantify the benefit of a treatment versus the risk of toxicity before theranostic Au nanocomplexes can be translated into clinically accepted strategies for cancer therapy.

Acknowledgments

We acknowledge the funding provided by the Outstanding Youth Foundation from the Department of Science and Technology, Jilin Province (Project Number: 20170520046JH); the Start-Up Research Grant Program from Jilin University (Project Number: 451160102052); the HAI-Novartis Fellowship Award from the Haematology Association of Ireland and Novartis Oncology; and the CNRS Lebanon GRP2015.

Disclosure

The authors report no conflicts of interest in this work.

References

1. Lee DE, Koo H, Sun IC, Ryu JH, Kim K, Kwon IC. Multifunctional nanoparticles for multimodal imaging and theragnosis. *Chem Soc Rev*. 2012; 41(7):2656–2672.
2. Ryu JH, Koo H, Sun IC, et al. Tumor-targeting multi-functional nanoparticles for theragnosis: new paradigm for cancer therapy. *Adv Drug Deliv Rev*. 2012;64(13):1447–1458.
3. Ahmed N, Fessi H, Elaissari A. Theranostic applications of nanoparticles in cancer. *Drug Discov Today*. 2012;17(17–18):928–934.

4. Lim EK, Kim T, Paik S, Haam S, Huh YM, Lee K. Nanomaterials for theranostics: recent advances and future challenges. *Chem Rev*. 2015;115(1):327–394.
5. Namiki Y, Fuchigami T, Tada N, et al. Nanomedicine for cancer: lipid-based nanostructures for drug delivery and monitoring. *Acc Chem Res*. 2011;44(10):1080–1093.
6. Doane TL, Burda C. The unique role of nanoparticles in nanomedicine: imaging, drug delivery and therapy. *Chem Soc Rev*. 2012;41(7):2885–2911.
7. Faraday M. The Bakerian Lecture: experimental relations of gold (and other metals) to light. *Philos T R Soc A*. 1857;147:145–181.
8. Turkevich J, Stevenson PC, Hillier J. A study of the nucleation and growth processes in the synthesis of colloidal gold. *Discuss Faraday Soc*. 1951;11:55–75.
9. Frens G. Controlled nucleation for the regulation of the particle size in monodisperse gold suspensions. *Nature*. 1973;241(105):20–22.
10. Khoury CG, Vo-Dinh T. Gold nanostars for surface-enhanced Raman scattering: synthesis, characterization and optimization. *J Phys Chem C Nanomater Interfaces*. 2008;2008(112):18849–18859.
11. Dreaden EC, Alkilany AM, Huang X, Murphy CJ, El-Sayed MA. The golden age: gold nanoparticles for biomedicine. *Chem Soc Rev*. 2012;41(7):2740–2779.
12. Vigderman L, Zubarev ER. Therapeutic platforms based on gold nanoparticles and their covalent conjugates with drug molecules. *Adv Drug Deliv Rev*. 2013;65(5):663–676.
13. Singhana B, Slattery P, Chen A, Wallace M, Melancon MP. Light-activatable gold nanoshells for drug delivery applications. *AAPS PharmSciTech*. 2014;15(3):741–752.
14. Chen W, Zhang S, Yu Y, Zhang H, He Q. Structural-engineering rationales of gold nanoparticles for cancer theranostics. *Adv Mater Deerfield*. 2016;28(39):8567–8585.
15. Brown KR, Lyon LA, Fox AP, Reiss BD, Natan MJ. Hydroxylamine seeding of colloidal Au nanoparticles. 3. Controlled formation of conductive Au films. *Chem Mater*. 2000;12(2):314–323.
16. Rahme K, Nolan MT, Doody T, et al. Highly stable PEGylated gold nanoparticles in water: applications in biology and catalysis. *RSC Adv*. 2013;3(43):21016–21024.
17. Sau TK, Pal A, Jana NR, Wang ZL, Pal T. Size controlled synthesis of gold nanoparticles using photochemically prepared seed particles. *J Nanopart Res*. 2001;3(4):257–261.
18. Niu JL, Zhu T, Liu ZF. One-step seed-mediated growth of 30–150 nm quasispherical gold nanoparticles with 2-mercaptosuccinic acid as a new reducing agent. *Nanotechnology*. 2007;18(32):7.
19. Perrault SD, Chan WCW. Synthesis and surface modification of highly monodispersed, spherical gold nanoparticles of 50–200 nm. *J Am Chem Soc*. 2009;131(47):17042.
20. Liu X, Xu H, Xia H, Wang D. Rapid seeded growth of monodisperse, quasi-spherical, citrate-stabilized gold nanoparticles via H_2O_2 reduction. *Langmuir*. 2012;28(38):13720–13726.
21. Foss CA, Hornyak GL, Stockert JA, Martin CR. Optical-properties of composite membranes containing arrays of nanoscopic gold cylinders. *J Phys Chem*. 1992;96(19):7497–7499.
22. Martin CR. Nanomaterials: a membrane-based synthetic approach. *Science*. 1994;266(5193):1961–1966.
23. Perez-Juste J, Pastoriza-Santos I, Liz-Marzan LM, Mulvaney P. Gold nanorods: synthesis, characterization and applications. *Coordin Chem Rev*. 2005;249(17–18):1870–1901.
24. Jana NR, Gearheart L, Murphy CJ. Evidence for seed-mediated nucleation in the chemical reduction of gold salts to gold nanoparticles. *Chem Mater*. 2001;13(7):2313–2322.
25. Nikoobakht B, El-Sayed MA. Preparation and growth mechanism of gold nanorods (NRs) using seed-mediated growth method. *Chem Mater*. 2003;15(10):1957–1962.
26. Skrabalak SE, Chen JY, Sun YG, et al. Gold nanocages: synthesis, properties, and applications. *Acc Chem Res*. 2008;41(12):1587–1595.
27. Yong KT, Sahoo Y, Swihart MT, Prasad PN. Synthesis and plasmonic properties of silver and gold nanoshells on polystyrene cores of different size and of gold-silver core-shell nanostructures. *Colloid Surf A*. 2006;290(1–3):89–105.
28. Oldenburg SJ, Averitt RD, Westcott SL, Halas NJ. Nanoengineering of optical resonances. *Chem Phys Lett*. 1998;288(2–4):243–247.
29. Pham T, Jackson JB, Halas NJ, Lee TR. Preparation and characterization of gold nanoshells coated with self-assembled monolayers. *Langmuir*. 2002;18(12):4915–4920.
30. Prodan E, Radloff C, Halas NJ, Nordlander P. A hybridization model for the plasmon response of complex nanostructures. *Science*. 2003;302(5644):419–422.
31. Kreibig U, Vollmer M. *Optical Properties of Metal Clusters*. Berlin Heidelberg: Springer-Verlag; 1995.
32. Cobley CM, Chen JY, Cho EC, Wang LV, Xia YN. Gold nanostructures: a class of multifunctional materials for biomedical applications. *Chem Soc Rev*. 2011;40(1):44–56.
33. Huang X, El-Sayed MA. Gold nanoparticles: optical properties and implementations in cancer diagnosis and photothermal therapy. *J Adv Res*. 2010;1:13–28.
34. Jain PK, Lee KS, El-Sayed IH, El-Sayed MA. Calculated absorption and scattering properties of gold nanoparticles of different size, shape, and composition: applications in biological imaging and biomedicine. *J Phys Chem B*. 2006;110(14):7238–7248.
35. Yguerabide J, Yguerabide EE. Light-scattering submicroscopic particles as highly fluorescent analogs and their use as tracer labels in clinical and biological applications – I. Theory. *Anal Biochem*. 1998;262(2):137–156.
36. Yguerabide J, Yguerabide EE. Light-scattering submicroscopic particles as highly fluorescent analogs and their use as tracer labels in clinical and biological applications – II. Experimental characterization. *Anal Biochem*. 1998;262(2):157–176.
37. Sokolov K, Follen M, Aaron J, et al. Real-time vital optical imaging of precancer using anti-epidermal growth factor receptor antibodies conjugated to gold nanoparticles. *Cancer Res*. 2003;63(9):1999–2004.
38. Orendorff CJ, Sau TK, Murphy CJ. Shape-dependent plasmon-resonant gold nanoparticles. *Small*. 2006;2(5):636–639.
39. Lee KS, El-Sayed MA. Dependence of the enhanced optical scattering efficiency relative to that of absorption for gold metal nanorods on aspect ratio, size, end-cap shape, and medium refractive index. *J Phys Chem B*. 2005;109(43):20331–20338.
40. Hauck TS, Chan WC. Gold nanoshells in cancer imaging and therapy: towards clinical application. *Nanomedicine (Lond)*. 2007;2(5):735–738.
41. Skrabalak SE, Au L, Lu X, Li X, Xia Y. Gold nanocages for cancer detection and treatment. *Nanomedicine (Lond)*. 2007;2(5):657–668.
42. Huang X, Neretina S, El-Sayed MA. Gold nanorods: from synthesis and properties to biological and biomedical applications. *Adv Mater*. 2009;21(48):4880–4910.
43. Tong L, Wei QS, Wei A, Cheng JX. Gold nanorods as contrast agents for biological imaging: optical properties, surface conjugation and photothermal effects. *Photochem Photobiol*. 2009;85(1):21–32.
44. Lee KS, El-Sayed MA. Gold and silver nanoparticles in sensing and imaging: sensitivity of plasmon response to size, shape, and metal composition. *J Phys Chem B*. 2006;110(39):19220–19225.
45. Chen J, Saeki F, Wiley BJ, et al. Gold nanocages: bioconjugation and their potential use as optical imaging contrast agents. *Nano Lett*. 2005;5(3):473–477.
46. Sun YG, Mayers BT, Xia YN. Template-engaged replacement reaction: a one-step approach to the large-scale synthesis of metal nanostructures with hollow interiors. *Nano Lett*. 2002;2(5):481–485.
47. Agasti SS, Rana S, Park MH, Kim CK, You CC, Rotello VM. Nanoparticles for detection and diagnosis. *Adv Drug Deliv Rev*. 2010;62(3):316–328.
48. Portales H, Saviot L, Duval E, et al. Resonance and composition effects on the Raman scattering from silver-gold alloy clusters. *Eur Phys J D*. 2001;16(1–3):197–200.

49. Amendola V, Scaramuzza S, Agnoli S, Polizzi S, Meneghetti M. Strong dependence of surface plasmon resonance and surface enhanced Raman scattering on the composition of Au-Fe nanoalloys. *Nanoscale*. 2014;6(3):1423–1433.
50. Juluri BK, Zheng YB, Ahmed D, Jensen L, Huang TJ. Effects of geometry and composition on charge-induced plasmonic shifts in gold nanoparticles. *J Phys Chem C*. 2008;112(19):7309–7317.
51. Brust M, Walker M, Bethell D, Schiffrin DJ, Whyman R. Synthesis of thiol-derivatized gold nanoparticles in a 2-phase liquid-liquid system. *J Chem Soc Chem Comm*. 1994;(7):801–802.
52. Sardar R, Funston AM, Mulvaney P, Murray RW. Gold nanoparticles: past, present, and future. *Langmuir*. 2009;25(24):13840–13851.
53. Guo J, Armstrong MJ, O'Driscoll CM, Holmes JD, Rahme K. Positively charged, surfactant-free gold nanoparticles for nucleic acid delivery. *RSC Adv*. 2015;5:17862–17871.
54. Chhour P, Naha PC, O'Neill SM, et al. Labeling monocytes with gold nanoparticles to track their recruitment in atherosclerosis with computed tomography. *Biomaterials*. 2016;87:93–103.
55. Liu XS, Huang N, Wang HB, Li H, Jin Q, Ji J. The effect of ligand composition on the in vivo fate of multidentate poly(ethylene glycol) modified gold nanoparticles. *Biomaterials*. 2013;34(33):8370–8381.
56. Conde J, Tian F, Hernandez Y, et al. In vivo tumor targeting via nanoparticle-mediated therapeutic siRNA coupled to inflammatory response in lung cancer mouse models. *Biomaterials*. 2013;34(31):7744–7753.
57. Shiao YS, Chiu HH, Wu PH, Huang YF. Aptamer-functionalized gold nanoparticles as photoresponsive nanoplatform for co-drug delivery. *ACS Appl Mater Interfaces*. 2014;6(24):21832–21841.
58. Arosio D, Chiodo F, Reina JJ, et al. Effective targeting of DC-SIGN by alpha-fucosylamide functionalized gold nanoparticles. *Bioconjugate Chem*. 2014;25(12):2244–2251.
59. Fitzgerald KA, Rahme K, Guo JF, Holmes JD, O'Driscoll CM. Anisamide-targeted gold nanoparticles for siRNA delivery in prostate cancer – synthesis, physicochemical characterisation and in vitro evaluation. *J Mater Chem B*. 2016;4(13):2242–2252.
60. Guo J, O'Driscoll CM, Holmes JD, Rahme K. Bioconjugated gold nanoparticles enhance cellular uptake: a proof of concept study for siRNA delivery in prostate cancer cells. *Int J Pharm*. 2016;509(1–2):16–27.
61. Shen S, Tang HY, Zhang XT, et al. Targeting mesoporous silica-encapsulated gold nanorods for chemo-photothermal therapy with near-infrared radiation. *Biomaterials*. 2013;34(12):3150–3158.
62. Guo JF, Ogier JR, Desgranges S, Darcy R, O'Driscoll C. Anisamide-targeted cyclodextrin nanoparticles for siRNA delivery to prostate tumours in mice. *Biomaterials*. 2012;33(31):7775–7784.
63. Fitzgerald KA, Malhotra M, Gooding M, et al. A novel, anisamide-targeted cyclodextrin nanoformulation for siRNA delivery to prostate cancer cells expressing the sigma-1 receptor. *Int J Pharm*. 2016; 499(1–2):131–145.
64. Stolik S, Delgado JA, Perez A, Anasagasti L. Measurement of the penetration depths of red and near infrared light in human "ex vivo" tissues. *J Photochem Photobiol B*. 2000;57(2–3):90–93.
65. Sakudo A. Near-infrared spectroscopy for medical applications: current status and future perspectives. *Clin Chim Acta*. 2016;455:181–188.
66. Henderson TA, Morries LD. Near-infrared photonic energy penetration: can infrared phototherapy effectively reach the human brain? *Neuropsych Dis Treat*. 2015;11:2191–2208.
67. El-Sayed IH, Huang X, El-Sayed MA. Surface plasmon resonance scattering and absorption of anti-EGFR antibody conjugated gold nanoparticles in cancer diagnostics: applications in oral cancer. *Nano Lett*. 2005;5(5):829–834.
68. Choi J, Yang J, Bang D, et al. Targetable gold nanorods for epithelial cancer therapy guided by near-IR absorption imaging. *Small*. 2012; 8(5):746–753.
69. Yang XM, Stein EW, Ashkenazi S, Wang LHV. Nanoparticles for photoacoustic imaging. *Wires Nanomed Nanobi*. 2009;1(4): 360–368.
70. Wang H, Brandl DW, Nordlander P, Halas NJ. Plasmonic nanostructures: artificial molecules. *Acc Chem Res*. 2007;40(1):53–62.
71. Halas NJ, Lal S, Chang WS, Link S, Nordlander P. Plasmons in strongly coupled metallic nanostructures. *Chem Rev*. 2011;111(6):3913–3961.
72. Li W, Chen X. Gold nanoparticles for photoacoustic imaging. *Nanomedicine (Lond)*. 2015;10(2):299–320.
73. Song JB, Yang XY, Jacobson O, et al. Ultrasmall gold nanorod vesicles with enhanced tumor accumulation and fast excretion from the body for cancer therapy. *Adv Mater Deerfield*. 2015;27(33):4910–4917.
74. Popovtzer R, Agrawal A, Kotov NA, et al. Targeted gold nanoparticles enable molecular CT imaging of cancer. *Nano Lett*. 2008;8(12): 4593–4596.
75. Liu H, Shen M, Zhao J, et al. Tunable synthesis and acetylation of dendrimer-entrapped or dendrimer-stabilized gold-silver alloy nanoparticles. *Colloids Surf B Biointerfaces*. 2012;94:58–67.
76. Jokerst JV, Lobovkina T, Zare RN, Gambhir SS. Nanoparticle PEGylation for imaging and therapy. *Nanomedicine (Lond)*. 2011;6(4): 715–728.
77. Zhou B, Yang J, Peng C, et al. PEGylated polyethylenimine-entrapped gold nanoparticles modified with folic acid for targeted tumor CT imaging. *Colloids Surf B Biointerfaces*. 2016;140:489–496.
78. Paul AM, Fan Z, Sinha SS, et al. Bioconjugated gold nanoparticle based SERS probe for ultrasensitive identification of mosquito-borne viruses using Raman fingerprinting. *J Phys Chem C*. 2015; 119(41):23669–23675.
79. Huang X, El-Sayed IH, Qian W, El-Sayed MA. Cancer cells assemble and align gold nanorods conjugated to antibodies to produce highly enhanced, sharp, and polarized surface Raman spectra: a potential cancer diagnostic marker. *Nano Lett*. 2007;7(6):1591–1597.
80. Hoejgaard L, Hesse B. Hybrid imaging: conclusions and perspectives. *Curr Med Imaging Rev*. 2011;7(3):252–253.
81. Meir R, Motiei M, Popovtzer R. Gold nanoparticles for in vivo cell tracking. *Nanomedicine (Lond)*. 2014;9(13):2059–2069.
82. Jin Y. Multifunctional compact hybrid Au nanoshells: a new generation of nanoplasmonic probes for biosensing, imaging, and controlled release. *Acc Chem Res*. 2014;47(1):138–148.
83. Zhao J, Wallace M, Melancon MP. Cancer theranostics with gold nanoshells. *Nanomedicine*. 2014;9(13):2041–2057.
84. Zhao Y, Pang B, Luehmann H, et al. Gold nanoparticles doped with (199) Au atoms and their use for targeted cancer imaging by SPECT. *Adv Healthc Mater*. 2016;5(8):928–935.
85. He XX, Liu FY, Liu L, Duan TC, Zhang HM, Wanq ZX. Lectin-conjugated Fe2O3@Au core@shell nanoparticles as dual mode contrast agents for in vivo detection of tumor. *Mol Pharm*. 2014;11(3): 738–745.
86. Huang S, Li C, Wang WP, et al. A54 peptide-mediated functionalized gold nanocages for targeted delivery of DOX as a combinational photothermal-chemotherapy for liver cancer. *Int J Nanomedicine*. 2017;12:5163–5176.
87. Zhang JM, Li C, Zhang X, et al. In vivo tumor-targeted dual-modal fluorescence/CT imaging using a nanoprobe co-loaded with an aggregation-induced emission dye and gold nanoparticles. *Biomaterials*. 2015;42:103–111.
88. Meir R, Shamalov K, Betzer O, et al. Nanomedicine for cancer immunotherapy: tracking cancer-specific T-cells in vivo with gold nanoparticles and CT imaging. *ACS Nano*. 2015;9(6):6363–6372.
89. Peng C, Zheng L, Chen Q, et al. PEGylated dendrimer-entrapped gold nanoparticles for in vivo blood pool and tumor imaging by computed tomography. *Biomaterials*. 2012;33(4):1107–1119.
90. Cheng B, He HC, Huang T, et al. Gold nanosphere gated mesoporous silica nanoparticle responsive to near-infrared light and redox potential as a theranostic platform for cancer therapy. *J Biomed Nanotechnol*. 2016;12(3):435–449.
91. Cheng Y, Dai Q, Morshed RA, et al. Blood-brain barrier permeable gold nanoparticles: an efficient delivery platform for enhanced malignant glioma therapy and imaging. *Small*. 2014;10(24):5137–5150.
92. Kim YH, Jeon J, Hong SH, et al. Tumor targeting and imaging using cyclic RGD-PEGylated gold nanoparticle probes with directly conjugated iodine-125. *Small*. 2011;7(14):2052–2060.

93. Sun IC, Eun DK, Koo H, et al. Tumor-targeting gold particles for dual computed tomography/optical cancer imaging. *Angew Chem Int Ed Engl*. 2011;50(40):9348–9351.
94. Chen Q, Li KA, Wen SH, et al. Targeted CT/MR dual mode imaging of tumors using multifunctional dendrimer-entrapped gold nanoparticles. *Biomaterials*. 2013;34(21):5200–5209.
95. Jing LJ, Liang XL, Deng ZJ, et al. Prussian blue coated gold nanoparticles for simultaneous photoacoustic/CT bimodal imaging and photothermal ablation of cancer. *Biomaterials*. 2014;35(22):5814–5821.
96. Gao S, Zhang LW, Wang GH, et al. Hybrid graphene/Au activatable theranostic agent for multimodalities imaging guided enhanced photothermal therapy. *Biomaterials*. 2016;79:36–45.
97. Chen WH, Yang CX, Qiu WX, et al. Multifunctional theranostic nanoplatform for cancer combined therapy based on gold nanorods. *Adv Healthc Mater*. 2015;4(15):2247–2259.
98. Jang B, Park JY, Tung CH, Kim IH, Choi Y. Gold nanorod-photosensitizer complex for near-infrared fluorescence imaging and photodynamic/photothermal therapy in vivo. *ACS Nano*. 2011;5(2):1086–1094.
99. Yang HW, Liu HL, Li ML, et al. Magnetic gold-nanorod/PNIPAAmMA nanoparticles for dual magnetic resonance and photoacoustic imaging and targeted photothermal therapy. *Biomaterials*. 2013;34(22):5651–5660.
100. Jokerst JV, Cole AJ, Van de Sompel D, Gambhir SS. Gold nanorods for ovarian cancer detection with photoacoustic imaging and resection guidance via Raman imaging in living mice. *ACS Nano*. 2012;6(11):10366–10377.
101. Guan T, Shang W, Li H, et al. From detection to resection: photoacoustic tomography and surgery guidance with indocyanine green loaded gold nanorod@liposome core-shell nanoparticles in liver cancer. *Bioconjug Chem*. 2017;28(4):1221–1228.
102. Karmani L, Labar D, Valembois V, et al. Antibody-functionalized nanoparticles for imaging cancer: influence of conjugation to gold nanoparticles on the biodistribution of 89Zr-labeled cetuximab in mice. *Contrast Media Mol Imaging*. 2013;8(5):402–408.
103. Xie H, Wang ZJ, Bao A, Goins B, Phillips WT. In vivo PET imaging and biodistribution of radiolabeled gold nanoshells in rats with tumor xenografts. *Int J Pharm*. 2010;395(1–2):324–330.
104. Chen W, Ayala-Orozco C, Biswal NC, et al. Targeting pancreatic cancer with magneto-fluorescent theranostic gold nanoshells. *Nanomedicine (Lond)*. 2014;9(8):1209–1222.
105. Coughlin AJ, Ananta JS, Deng NF, Larina IV, Decuzzi P, West JL. Gadolinium-conjugated gold nanoshells for multimodal diagnostic imaging and photothermal cancer therapy. *Small*. 2014;10(3):556–565.
106. Li L, Fu S, Chen C, et al. Microenvironment-driven bioelimination of magnetoplasmonic nanoassemblies and their multimodal imaging-guided tumor photothermal therapy. *ACS Nano*. 2016;10(7):7094–7105.
107. Chen HY, Li BW, Ren XY, et al. Multifunctional near-infrared-emitting nano-conjugates based on gold clusters for tumor imaging and therapy. *Biomaterials*. 2012;33(33):8461–8476.
108. Zhang P, Yang XX, Wang Y, Zhao NW, Xiong ZH, Huang CZ. Rapid synthesis of highly luminescent and stable Au-20 nanoclusters for active tumor-targeted imaging in vitro and in vivo. *Nanoscale*. 2014;6(4):2261–2269.
109. Croissant JG, Zhang D, Alsaiari S, et al. Protein-gold clusters-capped mesoporous silica nanoparticles for high drug loading, autonomous gemcitabine/doxorubicin co-delivery, and in-vivo tumor imaging. *J Control Release*. 2016;229:183–191.
110. Zhao YF, Sultan D, Detering L, Luehmann H, Liu YJ. Facile synthesis, pharmacokinetic and systemic clearance evaluation, and positron emission tomography cancer imaging of Cu-64-Au alloy nanoclusters. *Nanoscale*. 2014;6(22):13501–13509.
111. Hu H, Huang P, Weiss OJ, et al. PET and NIR optical imaging using self-illuminating Cu-64-doped chelator-free gold nanoclusters. *Biomaterials*. 2014;35(37):9868–9876.
112. Hu DH, Sheng ZH, Zhang PF, et al. Hybrid gold-gadolinium nanoclusters for tumor-targeted NIRF/CT/MRI triple-modal imaging in vivo. *Nanoscale*. 2013;5(4):1624–1628.
113. Han S, Samanta A, Xie X, et al. Gold and hairpin DNA functionalization of upconversion nanocrystals for imaging and in vivo drug delivery. *Adv Mater Deerfield*. Epub 2017 Mar 10;29(18).
114. Gao X, Yue Q, Liu Z, et al. Guiding brain-tumor surgery via blood-brain-barrier-permeable gold nanoprobes with acid-triggered MRI/SERRS signals. *Adv Mater*. Epub 2017 Mar 15;29(21).
115. Park J, Park J, Ju EJ, et al. Multifunctional hollow gold nanoparticles designed for triple combination therapy and CT imaging. *J Control Release*. 2015;207:77–85.
116. Tian M, Lu W, Zhang R, et al. Tumor uptake of hollow gold nanospheres after intravenous and intra-arterial injection: PET/CT study in a rabbit VX2 liver cancer model. *Mol Imaging Biol*. 2013;15(5):614–624.
117. Lu W, Melancon MP, Xiong C, et al. Effects of photoacoustic imaging and photothermal ablation therapy mediated by targeted hollow gold nanospheres in an orthotopic mouse xenograft model of glioma. *Cancer Res*. 2011;71(19):6116–6121.
118. Liu Y, Ashton JR, Moding EJ, et al. A plasmonic gold nanostar theranostic probe for in vivo tumor imaging and photothermal therapy. *Theranostics*. 2015;5(9):946–960.
119. Huang J, Guo M, Ke HT, et al. Rational design and synthesis gamma Fe2O3@Au magnetic gold nanoflowers for efficient cancer theranostics. *Adv Mater*. 2015;27(34):5049.
120. Hou W, Xia F, Alfranca G, et al. Nanoparticles for multi-modality cancer diagnosis: simple protocol for self-assembly of gold nanoclusters mediated by gadolinium ions. *Biomaterials*. 2017;120:103–114.
121. D'hollander A, Mathieu E, Jans H, et al. Development of nanostars as a biocompatible tumor contrast agent: toward in vivo SERS imaging. *Int J Nanomedicine*. 2016;11:3703–3714.
122. Wang Y, Liu Y, Luehmann H, et al. Evaluating the pharmacokinetics and in vivo cancer targeting capability of Au nanocages by positron emission tomography imaging. *ACS Nano*. 2012;6(7):5880–5888.
123. Bao CC, Beziere N, del Pino P, et al. Gold nanoprisms as optoacoustic signal nanoamplifiers for in vivo bioimaging of gastrointestinal cancers. *Small*. 2013;9(1):68–74.
124. Cheng K, Kothapalli SR, Liu HG, et al. Construction and validation of nano gold tripods for molecular imaging of living subjects. *J Am Chem Soc*. 2014;136(9):3560–3571.
125. Link S, El-Sayed MA. Shape and size dependence of radiative, non-radiative and photothermal properties of gold nanocrystals. *Int Rev Phys Chem*. 2000;19(3):409–453.
126. Link S, Furube A, Mohamed MB, Asahi T, Masuhara H, El-Sayed MA. Hot electron relaxation dynamics of gold nanoparticles embedded in $MgSO_4$ powder compared to solution: the effect of the surrounding medium. *J Phys Chem B*. 2002;106(5):945–955.
127. Link S, Ei-Sayed MA. Optical properties and ultrafast dynamics of metallic nanocrystals. *Annu Rev Phys Chem*. 2003;54:331–366.
128. Link S, Hathcock DJ, Nikoobakht B, El-Sayed MA. Medium effect on the electron cooling dynamics in gold nanorods and truncated tetrahedra. *Adv Mater*. 2003;15(5):393.
129. Riley RS, Day ES. Gold nanoparticle-mediated photothermal therapy: applications and opportunities for multimodal cancer treatment. Wiley interdisciplinary reviews. *Nanomed Nanobiotechnol*. 2017;9(4):e1449.
130. Huang XH, Jain PK, El-Sayed IH, El-Sayed MA. Gold nanoparticles: interesting optical properties and recent applications in cancer diagnostic and therapy. *Nanomedicine*. 2007;2(5):681–693.
131. Hwang S, Nam J, Jung S, Song J, Doh H, Kim S. Gold nanoparticle-mediated photothermal therapy: current status and future perspective. *Nanomedicine (Lond)*. 2014;9(13):2003–2022.
132. Huang X, Qian W, El-Sayed IH, El-Sayed MA. The potential use of the enhanced nonlinear properties of gold nanospheres in photothermal cancer therapy. *Lasers Surg Med*. 2007;39(9):747–753.

133. El-Sayed IH, Huang XH, El-Sayed MA. Selective laser photo-thermal therapy of epithelial carcinoma using anti-EGFR antibody conjugated gold nanoparticles. *Cancer Lett*. 2006;239(1):129–135.
134. Hleb EY, Hafner JH, Myers JN, et al. LANTCET: elimination of solid tumor cells with photothermal bubbles generated around clusters of gold nanoparticles. *Nanomedicine*. 2008;3(5):647–667.
135. Li Z, Huang P, Zhang X, et al. RGD-conjugated dendrimer-modified gold nanorods for in vivo tumor targeting and photothermal therapy. *Mol Pharm*. 2010;7(1):94–104.
136. Ke HT, Wang JR, Tong S, et al. Gold nanoshelled liquid perfluorocarbon magnetic nanocapsules: a nanotheranostic platform for bimodal ultrasound/magnetic resonance imaging guided photothermal tumor ablation. *Theranostics*. 2014;4(1):12–23.
137. Ayala-Orozco C, Urban C, Bishnoi S, et al. Sub-100nm gold nanomatryoshkas improve photo-thermal therapy efficacy in large and highly aggressive triple negative breast tumors. *J Control Release*. 2014;191:90–97.
138. Allison RR, Moghissi K. Photodynamic therapy (PDT): PDT mechanisms. *Clin Endosc*. 2013;46(1):24–29.
139. Schweitzer VG, Somers ML. PHOTOFRIN-mediated photodynamic therapy for treatment of early stage (Tis-T2N0M0) SqCCa of oral cavity and oropharynx. *Laser Surg Med*. 2010;42(1):1–8.
140. Vankayala R, Sagadevan A, Vijayaraghavan P, Kuo CL, Hwang KC. Metal nanoparticles sensitize the formation of singlet oxygen. *Angew Chem Int Ed Engl*. 2011;50(45):10640–10644.
141. Vankayala R, Lin CC, Kalluru P, Chiang CS, Hwang KC. Gold nanoshells-mediated bimodal photodynamic and photothermal cancer treatment using ultra-low doses of near infra-red light. *Biomaterials*. 2014;35(21):5527–5538.
142. Chen R, Wang X, Yao XK, Zheng XC, Wang J, Jiang XQ. Near-IR-triggered photothermal/photodynamic dual-modality therapy system via chitosan hybrid nanospheres. *Biomaterials*. 2013;34(33):8314–8322.
143. von Maltzahn G, Park JH, Agrawal A, et al. Computationally guided photothermal tumor therapy using long-circulating gold nanorod antennas. *Cancer Res*. 2009;69(9):3892–3900.
144. Sun XL, Huang XL, Yan XF, et al. Chelator-free Cu-64-integrated gold nanomaterials for positron emission tomography imaging guided photothermal cancer therapy. *ACS Nano*. 2014;8(8):8438–8446.
145. Zhang Z, Wang J, Nie X, et al. Near infrared laser-induced targeted cancer therapy using thermoresponsive polymer encapsulated gold nanorods. *J Am Chem Soc*. 2014;136(20):7317–7326.
146. Li XJ, Takashima M, Yuba E, Harada A, Kono K. PEGylated PAMAM dendrimer-doxorubicin conjugate-hybridized gold nanorod for combined photothermal-chemotherapy. *Biomaterials*. 2014;35(24):6576–6584.
147. Shi H, Ye XS, He XX, et al. Au@Ag/Au nanoparticles assembled with activatable aptamer probes as smart "nano-doctors" for image-guided cancer thermotherapy. *Nanoscale*. 2014;6(15):8754–8761.
148. Shao JX, Xuan MJ, Dai LR, Si TY, Li JB, He Q. Near-infrared-activated nanocalorifiers in microcapsules: vapor bubble generation for in vivo enhanced cancer therapy. *Angew Chem Int Edit*. 2015;54(43):12782–12787.
149. Luo CH, Huang CT, Su CH, Yeh CS. Bacteria-mediated hypoxia-specific delivery of nanoparticles for tumors imaging and therapy. *Nano Lett*. 2016;16(6):3493–3499.
150. Wang X, Wang H, Wang Y, et al. A facile strategy to prepare dendrimer-stabilized gold nanorods with sub-10-nm size for efficient photothermal cancer therapy. *Sci Rep*. 2016;6:22764.
151. Liu Y, Yang M, Zhang J, et al. Human induced pluripotent stem cells for tumor targeted delivery of gold nanorods and enhanced photothermal therapy. *ACS Nano*. 2016;10(2):2375–2385.
152. Ayala-Orozco C, Urban C, Knight MW, et al. Au nanomatryoshkas as efficient near-infrared photothermal transducers for cancer treatment: benchmarking against nanoshells. *ACS Nano*. 2014;8(6):6372–6381.
153. Li W, Zhang XJ, Zhou MJ, et al. Functional core/shell drug nanoparticles for highly effective synergistic cancer therapy. *Adv Healthc Mater*. 2014;3(9):1475–1485.
154. Hao YW, Zhang BX, Zheng CX, et al. The tumor-targeting core-shell structured DTX-loaded PLGA@Au nanoparticles for chemo-photothermal therapy and X-ray imaging. *J Control Release*. 2015;220(pt A):545–555.
155. Wang L, Yuan YY, Lin SD, et al. Photothermo-chemotherapy of cancer employing drug leakage-free gold nanoshells. *Biomaterials*. 2016;78:40–49.
156. Xuan M, Shao J, Dai L, Li J, He Q. Macrophage cell membrane camouflaged Au nanoshells for in vivo prolonged circulation life and enhanced cancer photothermal therapy. *ACS Appl Mater Interfaces*. 2016;8(15):9610–9618.
157. Nie LM, Wang SJ, Wang XY, et al. In vivo volumetric photoacoustic molecular angiography and therapeutic monitoring with targeted plasmonic nanostars. *Small*. 2014;10(8):1585–1593.
158. Gao YP, Li YS, Chen JZ, et al. Multifunctional gold nanostar-based nanocomposite: synthesis and application for noninvasive MR-SERS imaging-guided photothermal ablation. *Biomaterials*. 2015;60:31–41.
159. Wang ZZ, Chen ZW, Liu Z, et al. A multi-stimuli responsive gold nanocage-hyaluronic platform for targeted photothermal and chemotherapy. *Biomaterials*. 2014;35(36):9678–9688.
160. Piao JG, Wang LM, Gao F, You YZ, Xiong YJ, Yang LH. Erythrocyte membrane is an alternative coating to polyethylene glycol for prolonging the circulation lifetime of gold nanocages for photothermal therapy. *ACS Nano*. 2014;8(10):10414–10425.
161. Wang ZH, Sun JH, Qiu YQ, et al. Specific photothermal therapy to the tumors with high EphB4 receptor expression. *Biomaterials*. 2015;68:32–41.
162. Zhou JL, Wang ZH, Li QP, et al. Hybridized doxorubicin-Au nanospheres exhibit enhanced near-infrared surface plasmon absorption for photothermal therapy applications. *Nanoscale*. 2015;7(13):5869–5883.
163. Kang S, Bhang SH, Hwang S, et al. Mesenchymal stem cells aggregate and deliver gold nanoparticles to tumors for photothermal therapy. *ACS Nano*. 2015;9(10):9678–9690.
164. Chen M, Tang SH, Guo ZD, et al. Core-shell Pd@Au nanoplates as theranostic agents for in-vivo photoacoustic imaging, CT imaging, and photothermal therapy. *Adv Mater*. 2014;26(48):8210–8216.
165. Li L, Nurunnabi M, Nafiujjaman M, Lee YK, Huh KM. GSH-mediated photoactivity of pheophorbide a-conjugated heparin/gold nanoparticle for photodynamic therapy. *J Control Release*. 2013;171(2):241–250.
166. Zhang Y, Qian J, Wang D, Wang YL, He SL. Multifunctional gold nanorods with ultrahigh stability and tunability for in vivo fluorescence imaging, SERS detection, and photodynamic therapy. *Angew Chem Int Edit*. 2013;52(4):1148–1151.
167. Kim JY, Choi WI, Kim M, Tae G. Tumor-targeting nanogel that can function independently for both photodynamic and photothermal therapy and its synergy from the procedure of PDT followed by PTT. *J Control Release*. 2013;171(2):113–121.
168. Vankayala R, Huang YK, Kalluru P, Chiang CS, Hwang KC. First demonstration of gold nanorods-mediated photodynamic therapeutic destruction of tumors via near infra-red light activation. *Small*. 2014;10(8):1612–1622.
169. Wang BK, Wang JH, Liu Q, et al. Rose-bengal-conjugated gold nanorods for in vivo photodynamic and photothermal oral cancer therapies. *Biomaterials*. 2014;35(6):1954–1966.
170. Ye SF, Kang N, Chen M, et al. Tat/HA2 peptides conjugated AuNR@pNIPAAm as a photosensitizer carrier for near infrared triggered photodynamic therapy. *Mol Pharm*. 2015;12(7):2444–2458.
171. Srivatsan A, Jenkins SV, Jeon M, et al. Gold nanocage-photosensitizer conjugates for dual-modal image-guided enhanced photodynamic therapy. *Theranostics*. 2014;4(2):163–174.

172. Huang P, Lin J, Wang SJ, et al. Photosensitizer-conjugated silica-coated gold nanoclusters for fluorescence imaging-guided photodynamic therapy. *Biomaterials*. 2013;34(19):4643–4654.
173. Nair LV, Nazeer SS, Jayasree RS, Ajayaghosh A. Fluorescence imaging assisted photodynamic therapy using photosensitizer-linked gold quantum clusters. *ACS Nano*. 2015;9(6):5825–5832.
174. Broering R, Real CI, John MJ, et al. Chemical modifications on siRNAs avoid Toll-like-receptor-mediated activation of the hepatic immune system in vivo and in vitro. *Int Immunol*. 2014;26(1):35–46.
175. Longmire M, Choyke PL, Kobayashi H. Clearance properties of nano-sized particles and molecules as imaging agents: considerations and caveats. *Nanomedicine*. 2008;3(5):703–717.
176. Li W, Szoka FC Jr. Lipid-based nanoparticles for nucleic acid delivery. *Pharm Res*. 2007;24(3):438–449.
177. Guo JF, Bourre L, Soden DM, O'Sullivan GC, O'Driscoll C. Can non-viral technologies knockdown the barriers to siRNA delivery and achieve the next generation of cancer therapeutics? *Biotechnol Adv*. 2011;29(4):402–417.
178. Kumar A, Zhang X, Liang XJ. Gold nanoparticles: emerging paradigm for targeted drug delivery system. *Biotechnol Adv*. 2013;31(5):593–606.
179. Guo JF, Rahme K, Fitzgerald KA, Holmes JD, O'Driscoll CM. Biomimetic gold nanocomplexes for gene knockdown: will gold deliver dividends for small interfering RNA nanomedicines? *Nano Res*. 2015;8(10):3111–3140.
180. Chwalek K, Bray LJ, Werner C. Tissue-engineered 3D tumor angiogenesis models: potential technologies for anti-cancer drug discovery. *Adv Drug Deliver Rev*. 2014;79–80:30–39.
181. Quail DF, Joyce JA. Microenvironmental regulation of tumor progression and metastasis. *Nat Med*. 2013;19(11):1423–1437.
182. Beck B, Blanpain C. Unravelling cancer stem cell potential. *Nat Rev Cancer*. 2013;13(10):727–738.
183. Moghimi SM, Hunter AC, Andresen TL. Factors controlling nanoparticle pharmacokinetics: an integrated analysis and perspective. *Annu Rev Pharmacol*. 2012;52:481–503.
184. Zhou C, Long M, Qin YP, Sun XK, Zheng J. Luminescent gold nanoparticles with efficient renal clearance. *Angew Chem Int Edit*. 2011;50(14):3168–3172.
185. Hirn S, Semmler-Behnke M, Schleh C, et al. Particle size-dependent and surface charge-dependent biodistribution of gold nanoparticles after intravenous administration. *Eur J Pharm Biopharm*. 2011;77(3):407–416.
186. Alric C, Miladi I, Kryza D, et al. The biodistribution of gold nanoparticles designed for renal clearance. *Nanoscale*. 2013;5(13):5930–5939.
187. Simpson CA, Salleng KJ, Cliffel DE, Feldheim DL. In vivo toxicity, biodistribution, and clearance of glutathione-coated gold nanoparticles. *Nanomedicine*. 2013;9(2):257–263.
188. Zhang XD, Wu D, Shen X, Liu PX, Fan FY, Fan SJ. In vivo renal clearance, biodistribution, toxicity of gold nanoclusters. *Biomaterials*. 2012;33(18):4628–4638.
189. Khlebtsov N, Dykman L. Biodistribution and toxicity of engineered gold nanoparticles: a review of in vitro and in vivo studies. *Chem Soc Rev*. 2011;40(3):1647–1671.
190. Xie J, Lee S, Chen XY. Nanoparticle-based theranostic agents. *Adv Drug Deliver Rev*. 2010;62(11):1064–1079.
191. Hanahan D, Weinberg RA. Hallmarks of cancer: the next generation. *Cell*. 2011;144(5):646–674.
192. Xia Y, Li W, Cobley CM, et al. Gold nanocages: from synthesis to theranostic applications. *Acc Chem Res*. 2011;44(10):914–924.

International Journal of Nanomedicine

Dovepress

Publish your work in this journal

The International Journal of Nanomedicine is an international, peer-reviewed journal focusing on the application of nanotechnology in diagnostics, therapeutics, and drug delivery systems throughout the biomedical field. This journal is indexed on PubMed Central, MedLine, CAS, SciSearch®, Current Contents®/Clinical Medicine, Journal Citation Reports/Science Edition, EMBase, Scopus and the Elsevier Bibliographic databases. The manuscript management system is completely online and includes a very quick and fair peer-review system, which is all easy to use. Visit http://www.dovepress.com/testimonials.php to read real quotes from published authors.

Submit your manuscript here: http://www.dovepress.com/international-journal-of-nanomedicine-journal